6-2014

Electroplating of Nanoengineered Polymer Substrate

Brandon Voelker
Western Michigan University, bjvoelker@gmail.com

Follow this and additional works at: http://scholarworks.wmich.edu/masters_theses

Part of the Nanoscience and Nanotechnology Commons, and the Polymer and Organic Materials Commons

ELECTROPLATING OF NANOENGINEERED POLYMER SUBSTRATE

by

Brandon Voelker

A thesis submitted to the Graduate College
in partial fulfillment of the requirements
for the Degree of Master of Science in Engineering (Mechanical)
Mechanical and Aerospace Engineering
Western Michigan University
June 2014

Thesis Committee

Muralidhar Ghantasala, Ph.D, Chair
Daniel Kujawski, Ph.D, D.Sc.
HoSung Lee, Ph.D.

ELECTROPLATING OF NANOENGINEERED POLYMER SUBSTRATE

Brandon Voelker, M.S.E.

Western Michigan University, 2014

The development of a polyethylene based polymer with metallic inclusions, a nanoengineered polymer, has recently opened up great potential for many new commercial and industrial applications. The major advantage of developing these nanoengineered polymers is to be able to tailor the resistance and other properties by varying the composition of the polymer. The industrial usage of this polymer benefits from the addition of an electrically conductive, metallic coating. This research develops methods of electroplating nickel and copper layers on to the polymer substrates using DC and pulsed techniques.

Electroplating is conducted in a 1000 mL beaker using a specialized plating fixture with Nickel Sulfamate and Copper Acid as the electrolyte solutions for the nickel and copper films, respectively. The deposition duty cycles and cathodic current densities are varied to generate 24 unique samples. Examination of the electroplated coatings is completed utilizing Scanning Electron Microscopy (SEM), as well as nano-indentation analysis to measure mechanical properties.

The SEM analysis concluded the nickel film's exhibit a greater degree of porosity than the copper films, as a lack of nucleation site formation is noted early in the deposition process. SEM imaging also revealed the relative grain size of each parameter combination, of which copper films exhibit distinct, clear grain boundaries, whereas nickel films feature a smooth featureless topography. The Nanoindentation results concluded a positive correlation between an increase in the duty cycle and/or current density to an increase in hardness and Young's Modulus for both copper and nickel films. Copper films are found to exhibit a higher Young's Modulus and a lower hardness than the nickel films, across all electrodeposition parameters. These parameters are confirmed significant at a 95 percent confidence level as per an ANOVA statistical examination.

Acknowledgments

First and foremost I would like to extend my deepest gratitude to my thesis chair, Dr. Muralidhar K. Ghantasala, who has encouraged, supported, and challenged me throughout my research. He has been a continuing source of motivation and knowledge for which I am eternally grateful.

I would also like to thank my committee members Dr. Daniel Kujawski and Dr. HoSung Lee for their continued counsel throughout my studies and use of their lab equipment. I would like to thank Dr. Paul Engelmann for his immense insight and effort to manufacture the samples. I also wish to thank Mr. Jeff Wheeler for providing the basis for this research and his continued guidance.

Last but certainly not least I would like to thank my family and friends. My parents Ray and Jeanette who provided the means and unrivaled support for me to pursue my academic interests. My brother Justin and Sister-in-Law Megan who have always been my greatest source of inspiration and role models of character and excellence. And to my Fianceé Alyssa, for her unwavering daily support, compassion, and care throughout my graduate studies.

Brandon Voelker

Table of Contents

Table of Contents—Continued

List of Tables

List of Figures

List of Figures—Continued

Chapter 1

Introduction

1.1 Introduction

Materials dominate nearly every facet of our life. Evident by the classification of historical time frames by the material which had the most significant implications (Stone Age, Bronze Age, Iron Age, etc). Many have theorized which material will come to dominate our current society and mark our place in history. It is the opinion of the author ours will be known as the dawn of the smart materials.

Recent technological advancements have stimulated the research and development of new materials, as well as new processing techniques. For example the element Silicon was discovered in the early 19th century; however it wasn't until over a century later its characteristic usage came to fruition in the form of computer chips. Silicon is now almost exclusively used as the transistors and semi-conductor substrate upon which integrated circuits are formed. The basis of all modern computing systems, the integrated circuit, has inextricable linked silicon to our everyday lives.

Present day research and development pushes forward at a frenzied pace as new materials and processes are developed and examined. Existing elements are being re-imagined and re-engineered in the search to find the next life changing technological advancement. Carbon for example has been exemplified for its implications in a wide variety of markets, from brilliant diamond to the advent of the carbon nanotube and graphene which has presented engineers and scientists alike with a new organization structure of the carbon element that results in extraordinary physical properties. One such usage may come in the form of the replacement of the previously mentioned silicon for integrated circuit transistors. As digital circuits utilizing carbon nanotube transistors have the potential to present an increase in the energy efficiency of integrated circuits [1], Figure 1.1. Thus the next revolution of computers may be based on the nanointerconnect technologies utilizing these new methods.
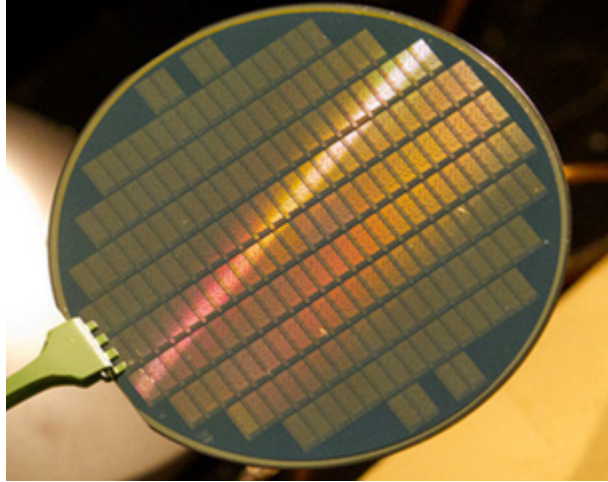
Figure 1.1: Computer developed at Sanford University consisting of 178 Transistors[2]

Existing products are also benefiting from new process development. Smart polymers utilizing capacitance properties act as sensors to measure automotive tire wear. Increasing the safety of passenger vehicles [3]. That same automobile may benefit from Carbon Fiber Reinforced Plastic (CFRP) components. The manufacturing of which includes a process of stranding together nearly 50,000 seven micron thick filaments [4] A process normal reserved for specialty racecar applications is now becoming commercially available due to advancements in CRFP forming technologies.

The fruition of commercial vehicles powered by hydrogen fuel cells may be the greatest innovation and achievement of this century. The most promising fuel cell, the Proton Exchange Membrane Fuel Cell (PEMFC), uses a thin film polymer electrolyte membrane as a basis for operation, Figure 1.2. The manufacturing of which has been revolutionized at Georgia Tech by directly coating the membrane onto the porous gas diffusion layer Figure 1.2. This eliminates the need for a sacrificial backing material which has been traditionally used in this process. This innovation reduces the number of required subsequent processing steps, saving time and money [5].
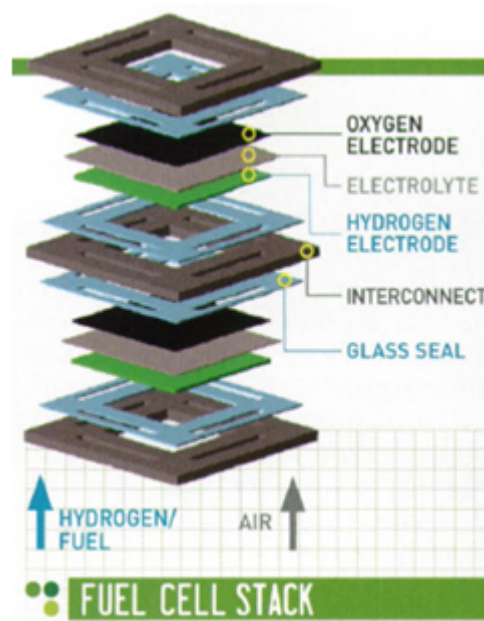
Figure 1.2: Typical Proton Exchange Membrane Fuel Cell Stack[5]

Manufacturing advancements, however, are not limited to automotive applications. Perhaps the most proliferate innovations come from the aeronautical and spacecraft sector. Manufacturing advancements such as the additive manufacturing of Ti-6Al-4V Alloys are pushing the envelope of complex componentry. Challenging engineers to rethink and reimaging the possibilities of machined and formed modules for spacecraft applications. The process involves a layer by layer deposition of the source material to form a component, directly from a CAD file [6].

The extraordinary research into new processes and materials has begun to blur the lines of the once well defined material property groups. The classification of conductor, semi-conductor, or insulator has been the prominent electrical characterization of a material. However new material adaptations and manufacturing processes have begun to de-organize classical knowledge of material capabilities. Polymers, such as polyethylene for example, are traditional insulators. Yet recent technological advancements in the processing of this polymer have resulted in the adaptation of a new variation of the polymer. A polymer with nano-scale metallic inclusions which can greatly alter the electrical properties from insulator, to conductor.

This research focuses on a polyethylene based nano-engineered polymer with selective resistance. Material properties from the supplier document the mechanical properties listed below, Table 1.1. In an effort to expand the potential applications of the material, electrical contacts are selected as a beneficial addition to the polymer. The electrical contacts would be of the form of a thin metallic film upon the polymer substrate. The application of a metallic layer on a polymer substrate has numerous engineering

Table 1.1: Mechanical Properties of Polymer

Tensile Modulus	3600 MPa
Flexural Modulus	3400 MPa
Izod Impact	8 kJ/m2
Thermal Conductivity	1.2 W/mK
Density	1.24 g/cm3

and product applications. While the nanoengineered polymer has a resistance of over 1000 Ohms, the addition of a metallic conductor can reduce the resistance to negligible levels in selective patterns. The strength to weight ratio and formability of polyethylene based polymers has resulted in an increase in their usage in the past few decades.

However, the inherent insulatory electrical property has limited their usage. The addition of the metallic layer coupled with the nano-scale metallic inclusions now opens this material to new markets where electrical conductivity is a requirement. An example of a product engineering application would be the back of a cellular phone cover integrated with the antenna. The polymer substrate will retain the current desired specifications of the cover, while a metallic coating could form the necessary pattern to serve as the phones antenna.

Metallic films deposited on semi-conductive polymeric substrates is not a well documented research field. Experiments conducted by Fleury Et. Al. [7] have presented deposition process to permit the electroplating of insulators with limited success. This research aims to bridge the gap between electroplating of conductors and insulators by theoretical and experimental research into the electrodeposition of various metals onto a nanoengineered polymer substrate.

1.2   Organization of the Thesis

The second chapter is presented as a literature review to the electroplating process and related technologies. The basic theories of electrodeposition will be discussed as well as an in-depth analysis regarding the existing research concerning the electrodepositon of a metallic film onto a polymeric substrate. An introduction to nanoindentation is presented as it is the primary means by which analytical results are derived. Specifically research into the special case of measuring properties of a film which have a higher Young's Modulus, then the substrate upon which it is formed.

The third chapter will examine the manufacturing methods used to form the polymeric substrates. Various equipment and processes will be highlighted that are used in the production of the substrates, both in rod and sheet form. Post forming operations to prepare the samples for electroplating are also discussed with relation to the optimization of electroplating parameters.

Throughout this research various simulations are preformed in parallel with the experimentation to aid in the understanding of various phenomena as well as a validation of theories and results. Chapter four covers the simulations completed utilizing various engineering software packages such as COMSOL Multiphysics as well as ANSYS. The simulations presented aid in the understanding of the effects of film porosity as it relates to stress distribution, as well as the optimization of parameters concerning nanoindentation experimentation.

The fifth chapter presents the electroplating parameters; including various current densities, electroplating durations, duty cycles, as well as materials, and their relationship to the optimization efforts. This chapter also covers the experemintal procedure and generation of the samples analyzed throughout the course of this research. Including the measurements recorded prior, during, and post deposition. The chapter concludes with the analysis and characterization of these samples. Various analytical methods are conducted on the samples such as SEM Imaging and Nanoindentation to determine critical mechanical and electrical properties. General trends of the measured properties are presented with respect to the deposition parameters and the optimization efforts. The results are examined by implementing an ANOVA statistical analysis to determine parameter significance.

Chapter six concludes the thesis with a review of the research conducted as well as the primary results. This provides a comprehensive analysis into the optimization of parameters pertaining to the electrodeposition of a metallic film onto a polymeric substrate. Further recommendations are then made relative to the advancement of research into this new field of study.

Chapter 2

Literature Review

2.1   Electroplating

This research focuses on the analysis of a copper or nickel layer deposited onto a nanoengineered polymer substrate, via various electroplating methods. Copper and nickel are chosen as the primary materials of interest due to their widespread use in the electroplating industry. Copper and nickel both encompass properties that lend themselves particularly well to the electroplating process. Specifically the ion mobility in solution permits these materials to be electroplated under a variety of circumstances and conditions with success. Additionally, both metals can be electroplated to form films that are corrosion resistant, ductile, and highly conductive [8]. Economic factors including cost, availability, etc also favor these metals in the electroplating industry.

Electroplating is a process in which an electric current is passed between two electrodes, an anode (positive electrode) and a cathode (negative electrode), separated by a solution. This solution is known as the electrolyte and must contain ions (electrically charged atoms or group of atoms) of the material to be plated [9]. With a current applied, electrons "flow" from the anode to the cathode. At the anode, the loss of electrons oxidizes the anode material and allows for the release of cations into the solution. These positively charged ions are drawn to the cathode where they are neutralized by the available electrons, reforming the constituent material as a solid deposit on the cathode.

The deposition of the metal onto the substrate occurs initially as a formation of nuclei. Once nucleation occurs, crystalline growth into a lattice structure takes place [10]. It is at this time the potential difference between the electrodes is likely to decrease in a galvanostatic method of electroplating (current is held constant, potential is free to vary as determined by Ohms Law). The method of crystalline growth is also determined by the current density. At higher current densities formation occurs more rapidly and it is less likely atoms of the depositing material will locate to a favorable site in the forming lattice.

Romankiw and O'Sullivan present a relationship between the normalized current (applied divided by maximum) and type of growth, Figure 2.1. From this figure it is shown low normalized current levels result in quality deposits while increasing the applied current to near the maximum results in poor quality, powdery deposits.
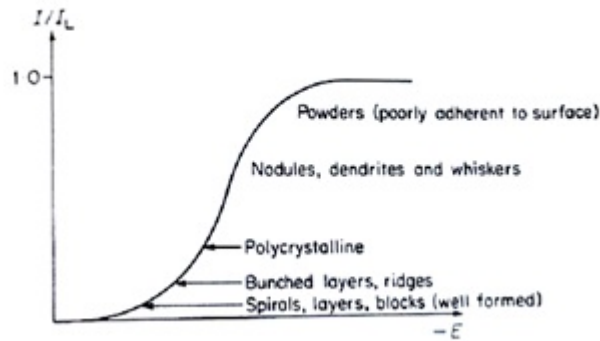
Figure 2.1: Normalized current compared to various electrodeposited characteristics[10]

A Watts-type bath is utilized for the nickel electroplating throughout this research. The Watts Nickel-Plating Bath is common throughout industry and research alike due to its high anode efficiency, quick deposition rates and tendency to produce ductile nickel film [8]. Nickel Sulfamate is used as the electrolyte with an average pH of 4.5. Nickel Sulfamate is chosen as the electrolyte as it has been shown to form deposits with relatively low stress (when compared to Nickel Sulfate). The temperature is held constant at 50 degrees celsius, agitation of the solution is provided via a magnetic stir-bar. The anode is a nickel plate suspended in the electrolyte. This plating system is expected to produce a nickel deposit with the following mechanical properties; Vickers hardness of 140-160, tensile strength of 350 MPa, and a 30% elongation in 5.08 cm [8].

Copper is electroplated using an Acid-Copper Bath. This electrolyte is chosen for its relatively high efficiency as well as rapid plating (compared to Copper Cyanide soultions which are typically restricted to striking due to the lower deposition rate). Acid-Copper Baths are heavily used in industry due to the ease at which a quality deposit can be achieved. This is primarily due to the 100% anode efficiency that copper achieves while in an acid solution [8]. In the course of this research copper acid solution will be used as the electrolyte at a temperature of 24 degrees celsius, while agitation of the solution is provided via a magnetic stir-bar. The anode is a copper plate suspended in the electrolyte.

Important theoretical calculations regarding the electroplating of metals include the application of Faraday's Law, presented in Equation 2.1. This relationship theorizes the mass of the material deposited (grams), to the applied current (amps), the plating time (hours), and the current efficiency. The constant

preceding the variables is a material dependant proportionality constant, equal to the atomic weight of the material divided by the product of the number of electrons in the electrochemical reaction and Faraday's constant (C = 1.0951 for Nickel, 1.1856 for Copper) [11]. The application of Faraday's Law will be utilized in this analysis for the calculation of current efficient, an important consideration in industrial applications.

$$m = CaIt \tag{2.1}$$

The deposition of nickel utilizing pulse techniques has been studied in previous investigations with regard to mechanical and morphological properties. One such study aimed to analyze nanocrystalline nickel deposits utilizing ultra narrow pulse width current [12]. In their research a magnetic pump fed the electrolyte solution between parallel plate cathode and anode plating system using a base nickel sulphamate bath solution. Both DC and pulse techniques were analyzed varying the current density from 20 to 4000 mA/cm^2. Using this process the thickness of each film was fixed at 100 microns and the surface morphology was examined by scanning electron microscopy and transmission electron microscopy [12].

The SEM results obtained indicate that with a pulse deposition on time of 10 microseconds and off time of 90 micro seconds the 1000 and 2000 mA/cm^2 deposits featured a similar topology, whereas at a peak current density of 3000 mA/cm^2 the grain size has been reduced and the grains themselves are more homogeneous [12]. This notion was continued by the experimental determination that higher current densities produced a finer grain size. Hardness values were also measured using a micro hardness tester with a loading force of 25 g. The results from which pose an interesting phenomenon, the pulse deposited samples feature hardness on the order of two times greater than those samples deposited by DC, Figure 2.2. Also the trend for increasing current density does not appear linear, as initial increases in current density increase the hardness. Until the current density reaches a value around 100 to 150 mA/cm^2 where the trend reverse, and the hardness steadily decreases [12].
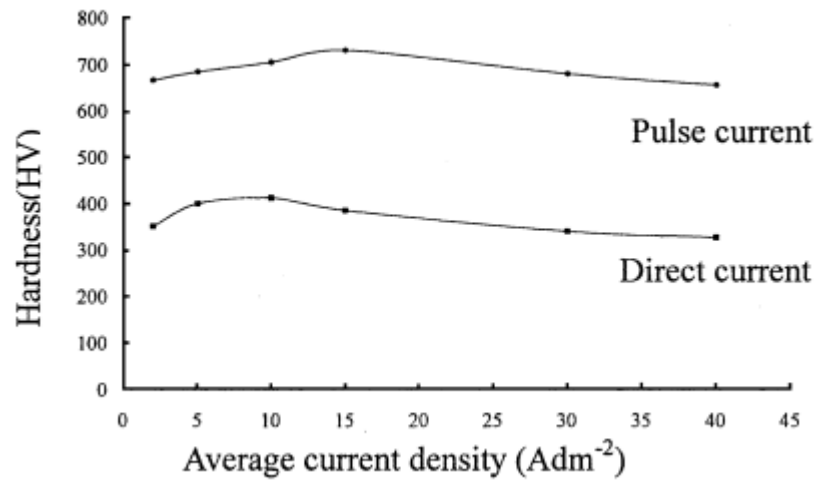
Figure 2.2: Hardness Date for Pulse and DC Deposited Samples[12]

One such explanation of these findings results from the effect of porosity in the measurements, in which it is claimed the porosity of the deposit reduces the hardness, and that porosity increases with an increase in current density [12]. While this research has presented excellent work regarding the effects of pulse versus DC methods of deposition on the microstructure and hardness of the deposits. The ranges of values used are not consistent with the desired outcome of the research presented in this Thesis, namely the 100 micron thick film and high current densities. Additionally, measurements regarding hardness and Young's Modulus of the film should be taken at such a fine level that the effects or porosity are not introduced, limiting the measurements to include only values derived from the constituent film material itself.

Electroplating of insulatory and semi-conductive substrates represents a field of research that has endured various levels of success. Industrial practices of electroless copper deposition have utilized Palladium catalyzed substrates in a multistep complex operation. Additionally, this particular method requires many hazardous solutions, including known carcinogens [13]. A research team from Greece presented findings in 2006 that claimed to solve this issue.

The research team from the National Technical University of Athens presented a method utilizing a conductive polymer (pyrrole) as a precoat. This electrically conductive layer deposited onto insulatory substrates, such as ABS, allowed for the future deposition of copper. Through the optimization of several parameters the team was able to reach a constant deposition rate of 0.0030 mg/min [13]. While this research presented a feasible alternative to the current methods, it still relied on a multistep operation including etching with $(NH4)2S2O8$ [13], thus limiting its industrial practicality.

Successful electroplating of insulators has also been realized by the usage of an electrode in contact

with the substrate to be plated, Figure 2.3. This technique depends on the outward propagation of the deposited material originating at the contact point of the electrode with the substrate [7]. Optimization efforts have lead to the controllability of grain size, thickness and growth speed, however there remain disadvantages. This method yields a slow rate of deposition and great effort must be used to control thickness to avoid the tendency of the film thickness to taper off as the distance from the electrode contact point increases.
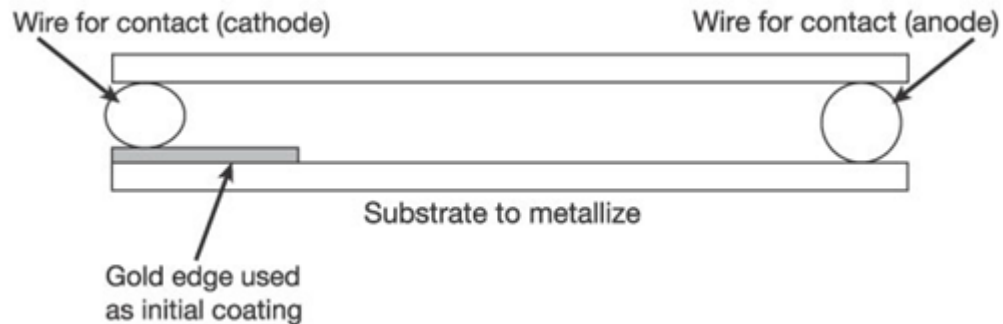
Figure 2.3: Electrode in contact with the substrate to be plated with gold seed area[7]

Research conducted by Ghantasala and Sood aimed to electroplate on a selectively resistive (2–20 ohm-cm) silicon wafer without the need for a base film [14]. Their methodology consisted of ion implantation on the face of the silicon to induce selective seeding. Utilizing a Metal Vapour Vacuum Arc ion implanter, 19 keV Pd^+ ions are implanted at various dosage levels. Permalloy is chosen as the electroplated material (for its widespread usage as a magnetic material in micro electromechanical structures) and in an effort to deposit high aspect ratio patterns; photoresist coupled with a contact mask aligner is used to form the patterns [14].

In conventional plating technologies of this type the seed layer is required to provide the initial conductive areas to allow for nucleation sites among the eventual deposits (this requires reforming of the photo resist mask). Whereas with the ion implantation method the original photoresist mask can be sustained throughout the electroplating process, decreasing time and complexity. The results of this research concluded that to form a continuous electroplated film on the silicon surface, an ion implantation dosage level between 1e16 and 1e17 ions/cm^2 is required [14].

Moreover a distinct boundary is formed, Figure 2.4, between the areas that received implantation and those that did not. The absence of any permalloy deposits in the region without ion implantation indicate the importance of ions on the substrate surface and their purpose of inducing nucleation sites (eventually evolving into continuous plating). The deposited films were examined for electrical resistance in which it was found increasing the implantation dose decreases the resistance. Additionally the films passed the scotch tape test indicating good adhesion [14]. This research presents a critical determination

in the ability for nucleation to occur on a semi-conductive substrate surface and the importance of ions at that surface.
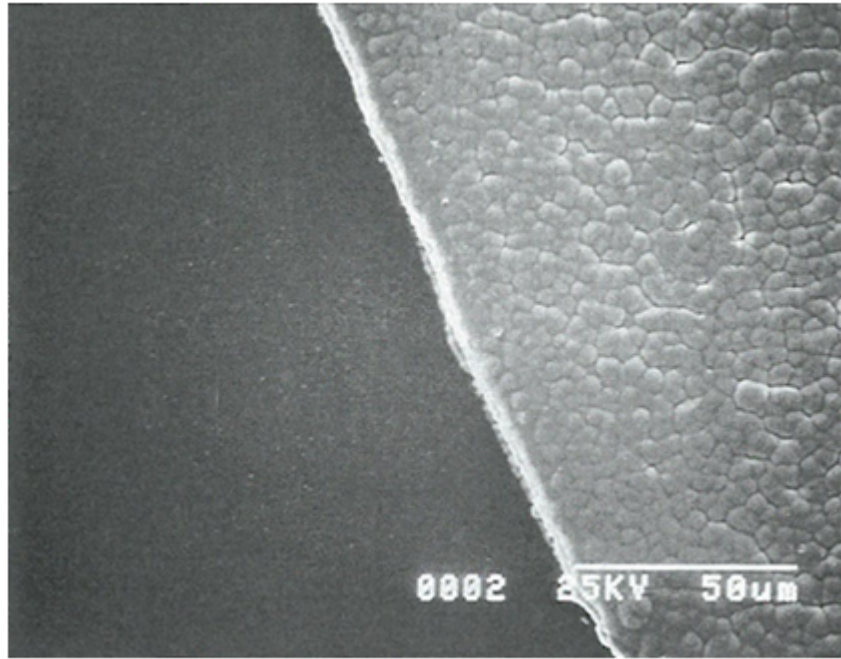
Figure 2.4: Interface between Unimplanted (left) and Implated (right) Surfaces[14]

Further research by Ghantasala and Sood examined that effects of ion implantation of Antimony on a silicon substrate, and the effects of various levels of annealing [15]. Wherein the technique of "backplating" is utilized on the reverse face (the face opposite of where plating will occur) of the substrate to serve as a cathode. Sb ions are selected in this research for their high standard electrode potential, which also has the opposite sign of the Pd ions [15]. Additionally, as Antimony forms an n-type dopant in Silicon, thermal annealing of the Pb ions can make them highly conductive [15]. The experimental procedure consisted of the ion implantation via a MEVVA implanter at 10 keV for Sb. Portions of the wafer are masked to separate regions of implanted and non-implanted. Variations of dosing are applied at regions around the substrate to study the effects of each dose. In the last step before electroplating some of the samples undergo a thermal annealing process to achieve electrical activation of the Antimony in the Silicon. Electroplating is carried out at 6 mA/cm^2 using a Nickel-Iron electrolyte bath to form a permalloy deposit [15].

The results of this experimentation reveled a "negative" effect as a result from the ion implantation in the samples that did not undergo annealing [15]. In which the regions that received ion implantation do not receive plating. In fact the only plating found on the substrate occurred in the unimplanted areas and can be classified as "stray" plating. The samples that underwent the annealing operation featured

a bright and continuous film over the implanted region. This phenomenon was observed for the doses of $5E12/cm^2$, $5E13/cm^2$, and $1E14/cm^2$ after 3 minutes of plating. The other doses at this time featured discontinuous films, however, after 30 minutes of plating all doses featured a continuous deposit [15]. This process proved fruitful for silicon substrates with a resistance of 1-3 ohm-cm. In the case of the nanoengineered polymer studied in this Thesis, the resistance of the substrate is over 1000 ohm-cm, as such this process is not a viable option. Yet is does provide more insight into the inherent characteristics of the nucleation process and how it can be achieved though masking techniques.

The nature of this research aims to bridge the existing gap between the electroplating of insulators and the electroplating of conductors. By use of a nanoengineered polymer substrate, various parameters will be examined and optimized to best determine the suitable electrodeposition conditions to depoist an ideal film. Ideal is defined in this context as a deposited film with superior adhesion, mechancial properties (Young's Modulus and Hardness), and electrical properties (low resistance). A review of relevant research concerning this topic has outlined the initial direction of research and provided insight into probable theories regarding optimization efforts. To measure the mechanical properties of the films, a specialized indentation system will be utilized to preform instrumented indentations on the deposits. The basic theory of which is covered in the following section.

2.2   Nanoindentation

Indentation analysis is one of the most common methods for measuring the mechanical properties of a material. Nanoindentation refers to the instrumented indentation measurement of small volumes of materials, first developed in the 1970s [16]. Since its inception nanoindentation has been used to characterize fracture mechanics of ceramics, mechanical behavior of thin films, residual stresses, as well as time dependent properties of materials [17]. A typical instrumented indentation set-up consists of a sharp tip penetrating the surface of the material to be measured, Figure 2.5. The penetration of the tip can typically be controlled via depth limitations (either nanometers or micrometers) or by maximum force (millinewtons). Electromagnetic or electrostatic actuation are the primary methods of force application while capacitive sensors are typically used to measure tip displacement [17].
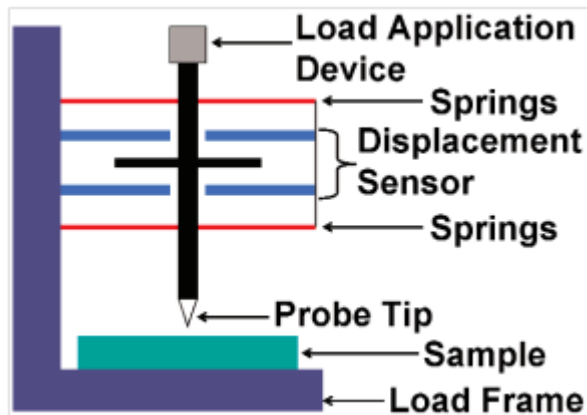
Figure 2.5: Typical schematic illustrating a nanoindentation instrumented indentation system[17]

The initial application of nanoindentation involved the following assumptions based on Sneddon's solution; infinitely large incompressible specimen, and an infinitely sharp indenter tip [16]. The obvious violation of these assumptions has lead to many proposed methods of mechanical property derivation. Initiated by the work of researchers at the Baikov Institute of Metallurgy, Doerner and Nix proposed a method to relate the force depth data to the contact area, assuming the change in area with depth was small (flat punch tip geometry) [18]. More recently research by Oliver and Pharr lead to the classification of contact solutions for many tip geometries, following the power law given in Equation 2.2. This power law is used to predict unloading data in an elastic contact indentation (P is the indenter load, h is the displacement of the indenter tip, α and h are constants) [18].

$$P = \alpha h^m \tag{2.2}$$

This theory was applied to determine the contact area, even if the area changed under unloading conditions (elastic deformation). Again with the application of Sneddon's solution Oliver and Pharr developed Equation 2.3 [18]. relating contact depth to area for an indentation. In this equation h_c is contact depth, h_{end} is maximum depth, θ is indenter geometry constant, P_{max} is maximum force, and S is the slope of the unloading profile [18]. This allows for the calculation of Young's Modulus as well as hardness for the sample being measured. A typical measurement profile is given in Figure 2.6

$$h_c = h_{end} - \theta \frac{P_{max}}{S} \tag{2.3}$$
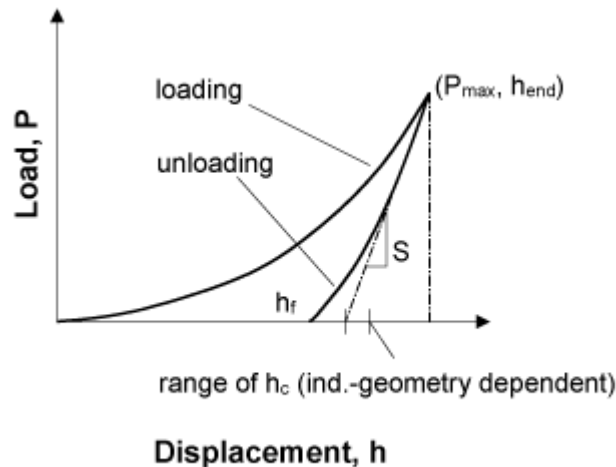
Figure 2.6: Typical loading and unloading profile of an indentation measurement[18]

Throughout this analysis the parameters of the nanoindentation experimentation are held constant at optimized values, resulting in the most accurate and precise values for indentation modulus as well as hardness. Such parameters include the loading profile, the indenter approach speed, the percent delta slope for contact determination, loading and unloading rates, and maximum depth. These parameters have been thoroughly investigated with respect to this specific analysis of a thin metallic film on a nanoengineered substrate.

The determination of the indentation modulus and hardness is calculated by the indentation software, using the aforementioned theory. The indentation hardness (HIT) is the measure of the samples resistance to plastic deformation. It is calculated by Equation 2.4, in which hardness is a function of the maximum force and the projected area which is a function of the indentation depth [19].

$$H_{IT} = \frac{F_{max}}{A_p} \tag{2.4}$$

The determination of the indentation modulus encompasses several equations, the first of which is the determination of the reduced modulus. E_r, Equation 2.5. The reduced modulus is a function of the unloading slope, indenter tip geometry, projected area, and contact depth [19].

$$E_r = \frac{\sqrt{\pi}S}{2\beta\sqrt{A_p h_c}} \tag{2.5}$$

From the reduced modulus the software calculates the plane strain modulus, E*, Equation 2.6 [19]. Which includes material properties of the indenter tip (diamond in this research); elastic modulus,

$E_i = 1141 GPa$, and poisson's ratio, $v = .07$.

$$E^* = \frac{1}{\frac{1}{E_r} - \frac{1-\nu_i^2}{E_i}}$$

(2.6)

Using the reduced modulus, the plane strain modulus, and an estimation of the sample's Poisson's ratio, v_s, the indentation modulus, E_{IT}, can be determined using Equation 2.7 [19].

$$E_{IT} = E^*(1 - \nu_s^2)$$

(2.7)

Most research into instrumented indentation of a film on a substrate falls into the category of a relatively softer film compared to the substrate. However this research involves the derivation of mechanical properties of a relatively harder film, compared to the substrate. As such deformations of the substrate may occur during film penetration, skewing the data. Even with a harder substrate one of the primary concerns of evaluating film properties is to distinguish the mechanical property contributions of the film from that of the substrate [20]. This difficulty is compounded when the substrate is softer.

Numerous techniques have been developed in an attempt to separate the effects of the substrate and the film. Such research has resulted in the general formula presented in Equation 2.8 [20], relating the effects of the substrates hardness, H_s, the film's hardness, H_f, and the compound hardness, H_c, to a function of the contact depth divided by the film thickness, α hc/t.

$$\frac{H_C - H_S}{H_F - H_S} = \alpha \frac{h_C}{t}$$

(2.8)

The theoretical model developed by Jonsson and Hogmark presents a function with fixed value parameters, such that a unique equation can be used [20]. The function is given by Equation 2.9 [20], where d is diagonal of the Vickers indentation and D is a constant relating to cracking of the film.

$$\alpha = 2D\frac{t}{d} - D^2\frac{t}{d}^2$$

(2.9)

Experimental data has shown inaccuracies of this model primary due to the assumption that the mechanical properties present a unique function for alpha, of which they do not. Data has shown factors such as mechanical properties of the film and substrate as well as the physical geometry of the indention has an effect on the weighting function [20]. As such the Korsunsky model was developed to fit experimental data, including factors such as relative contact indentation depth, Equation 2.10 [20]. In

the Korsunsky model k is dimensionless parameter relating the film thickness to the fracture toughness.

$$\alpha = \frac{1}{1 + k\frac{h_C}{t}^2} \tag{2.10}$$

One of the simplest methods for eliminating substrate effects when measuring film properties is to limit the indentation depth. Experimental data has shown if the ratio of film thickness divided by the contact indentation depth is greater than six, deformation is localized to the film [20]. However, this is a generalized statement and does not factor in the ratio of substrate hardness to film hardness. The primary disadvantage with implementing a minimal depth approach is the decrease in accuracy of the measured properties. As tip imperfections and surface topology have an increasing effect with shallower penetration depths.

A thorough review of previously completed research in the field of electroplating (specifically electroplating insulators) provides for an initial parameter selection as a starting point. Examination of successful and problematic conditions as encountered by previous research teams aids in the understanding of current and future results while providing a framework of interactions for the electroplating process. Instrumented indentation will be utilized for quantitative measurements of basic film properties such as hardness and Young's Modulus. An understanding of the physics and mathematics used to derive the results from an indentation measurement are critical to apply and understand the data. Especially concerning the important characteristic of these measurements as they are derived from a film located atop a relatively softer substrate.

Chapter 3

Manufacturing of Polymer Samples

The nanoengineered polymer resin ships from the manufacture as a polymeric bead. All subsequent forming operations are preformed at Western Michigan University's plastics lab. The thermoplastic nature of the polymer lends itself to many forming operations. Elevated temperature extrusion is chosen as the primary method of forming for the samples highlighted in this chapter, due to the ease of manufacturing and also the various output geometries that can be achieved. It is crucial during the forming stage that the parameters are selected such that the dispersion of the metallic inclusions in the polymer (that contribute to its semi-conductive nature) are not adversly effected [21] [22]. The first sets of samples analyzed are manufactured into a cylindrical shape. The final sets are manufactured into sheets to enhance the analytical capabilities.

3.1   Extruded Rod Samples

The productions of the first samples from the polymer resin are processed using a 3.175 cm Killion Extruder with a rod die. This produced a continuous rod with a nominal diameter of 3 mm. The samples were observed to be highly brittle with a porous surface. To prepare the samples for experimentation, the continuous rod was cut into segments 10 cm long, Figure 3.1. The samples were cleaned with acetone to remove any process contamination and placed inside test tubes.

Figure 3.1: Extruded Rod Polymer Sample

3.2 Extruded and Compressed Sheet Samples

To further explore the manufacturing possibilities of the polymer resin, the next set of samples are produced in two stages. In the first stage the polymeric beads are feed into a 3.175 cm inch Klein Extruder with a coat-hanger type sheet die at Western Michigan University, Figure 3.2. The specimen is extruded in a continuous sheet 13 centimeters wide. Every 15 centimeters a cut is made to separate the sample into discrete units.
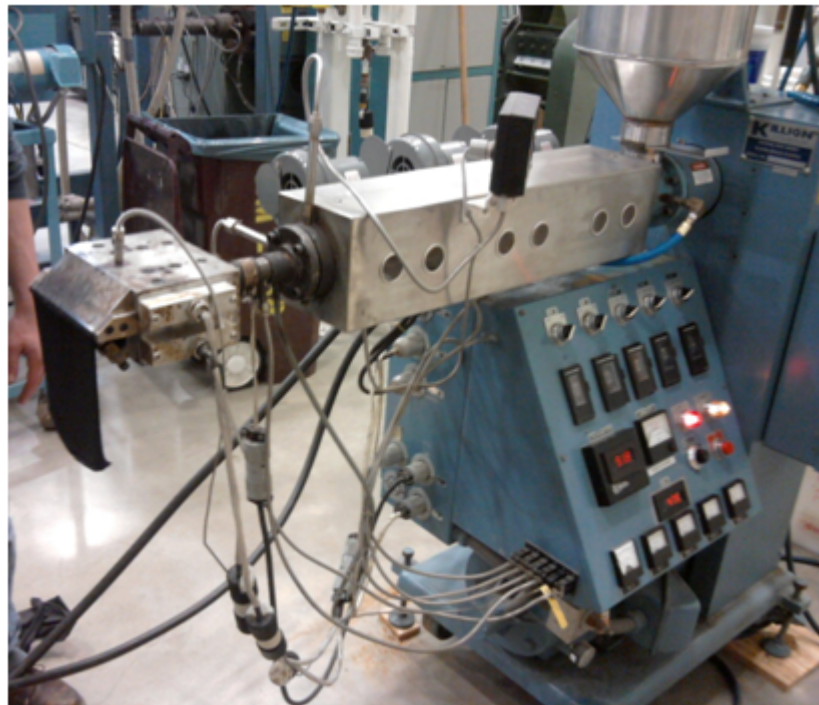
Figure 3.2: 1.25 inch Klein Extruder with a Coat-Hanger type Sheet Die

The sample sheet is then transferred to the compression stage, in an effort to provide a consistent

surface finish. The sample plaques are formed via a P-20 Steel and Ampco 940 SiNiCrCu compression mold, Figure 3.3, which are then placed into a 222,000 Newton Drake Compression Molding Press, Figure 3.4. During this compression process the sample is subjected to 133,500 Newtons of force for 60 seconds. The result is a sheet with a thickness of .7 mm. It is observed after the compression stage the ductility and resistance to fracture (compared to non-compression molded samples) has increased.
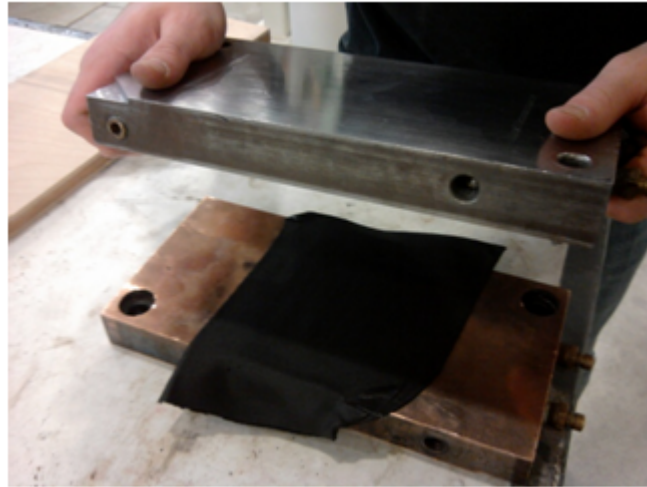
Figure 3.3: Warm Sample inserted between the Mold Halves

Figure 3.4: 25 Ton Drake Compression Molding Press

During the optimization process several parameters are varied with various levels of success. During this time the process is refined to promote successful sheet sample production. Initial conditions yielded unsatisfactory samples with inconsistent and damaged surface conditions, Figure 3.5. This presents the importance of optimization of parameters to manufacture a quality sample to be used in this analysis.

Figure 3.5: Poor Performance Sheet Sample

Once Optimized, the surface finish of the sheet, post-compression molding was determined sufficient. However it is desired to explore other manufacturing possibilities in an effort to develop a robust process. Thus a rolling operation is examined to determine its validity as a forming operation, as well as its effect on the surface finish. As such the samples are fed from the extruder directly into a Killion Extruders Three-Roll Mill, Figure 3.6.
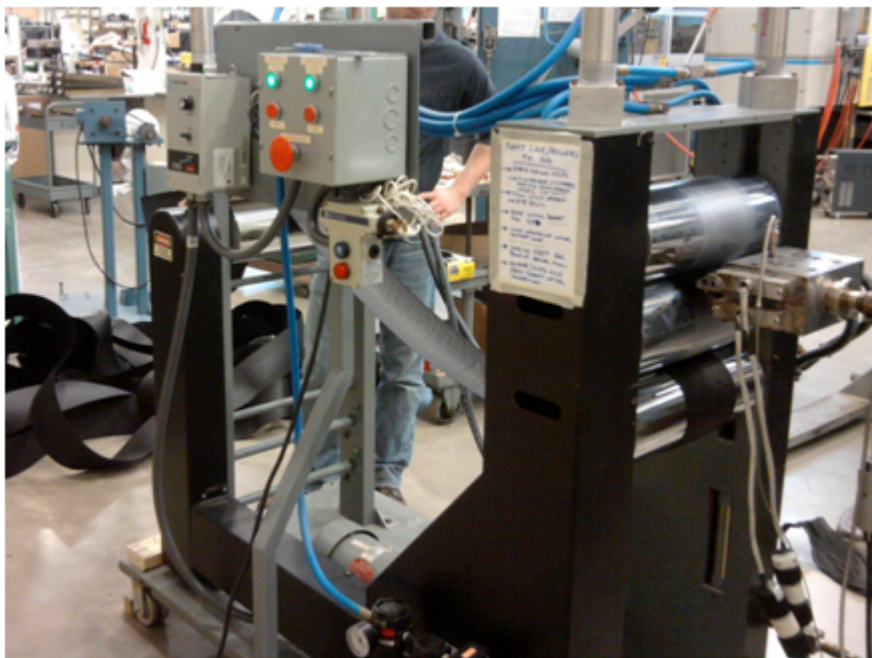
Figure 3.6: Extrudate being fed into the 3-Roll Mill

This process utilizing rolling compression of the sample greatly reduces the sample generation time as a continuous sheet can be formed without the need for individual, discrete, compression stages. However, optimization of the extruder/roller system can be difficult as it is required for the rollers to match the extrudate velocity exactly, or tearing may result. Additionally, the cooling of the polymer must be carefully controlled as it traverses through the rollers to preserve the composition of the inclusions [23]. The resulting sheet samples, Figure 3.7, are found to have a similar surface finish and thickness as those samples that were compression molded.

Figure 3.7: Compression Molded Polymer Sheet Sample

To provide an electrical contact to the negative terminal of the power supply during the electroplating process, the rod polymer samples underwent a vacuum deposition operation to partially coat the rod in an aluminum coating. The equipment used to perform the vacuum deposition is a Hitachi HUS-4 Evaporator, Figure 3.8. The Hitachi HUS-4 Evaporator System at Western Michigan University is capable of producing pressures down to 10-4 Torr and a continuous DC current of 0 to 140 Amperes.

Figure 3.8: Hitachi HUS-4 Evaporator at Western Michigan University

Samples are prepared for vacuum deposition by masking 70 mm of the samples length in an aluminum mask while leaving the remaining 30 mm exposed. Within the vacuum chamber a 20 gauge tungsten wire with a loop is spanned across the contacts of the DC current source. Aluminum wire with a .25 mm diameter is wound around the tungsten wire. The rod is than positioned in the vacuum chamber such that the exposed area of the rod is located in the geometric center of the loop in the tungsten wire, Figure 3.9.
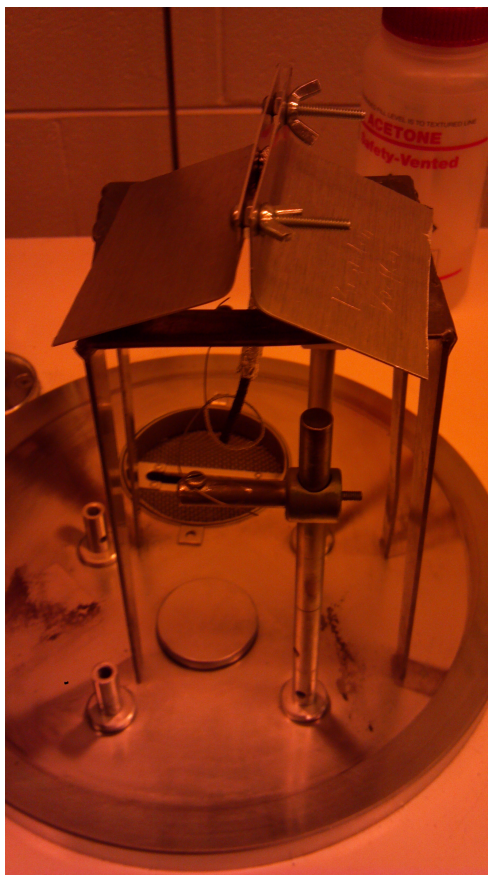
Figure 3.9: Sample positioned in the Vacuum Chamber

The chamber is locked and the vacuum is engaged decreasing the pressure within the chamber. Once the pressure has stabilized a current of 20 Amperes is passed through the tungsten wire. Joule heating results in a thermal energy transfer to the aluminum wire, causing the aluminum located on the tungsten to evaporate and attach to the rod sample. This produces a semi-coated aluminum rod as in Figure 3.10.

Figure 3.10: Rod Sample after Aluminum Deposition

For the compression molded/rolled polymer sheet samples the aluminum vacuum deposition was not conducted as it was determined the decrease in distance between the area to be plated and the connection to the negative terminal of the power supply (originally 25 mm with the rod samples reduced to .7 mm with the sheet samples) negated the effects of the aluminum coating. To prepare the samples

for electroplating 50 mm diameter circles were cut from the polymer sheets to create substrate wafers that could then fit within the wafer electroplating fixture, Figure 3.11. The samples were cleaned with acetone to remove any contamination from the forming process.
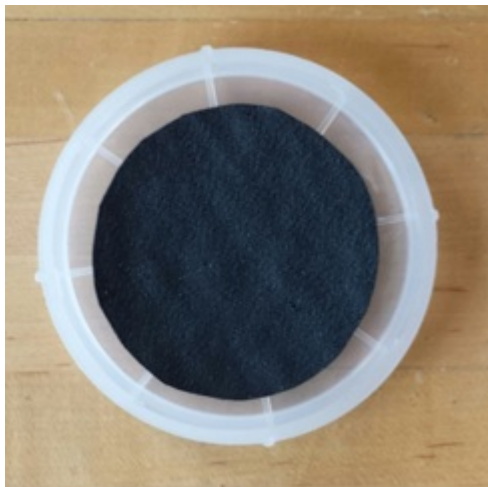
Figure 3.11: Polymer Wafer samples cut from Extruded and Rolled Sheets

The extrusion of the polymer occurs at a temperature greater than that of the polymer's melting temperature. Thus the polymer enters the die in a molten state. Within the die the polymer is deformed into the primary shape, and as it begins to cool recrystallization occurs. As polyethylene can be considered semi-crystalline the rate at which the polymer is cooled can have a significant impact on the morphology and physical/mechanical properties of the extrudate. Slow cooling allows for a longer period of position of the molecules and thus results in an extrudate with a lower specific volume. Rapid cooling forces the extrudate past the glass transition region at a higher temperature, resulting in a higher specific volume [24]. Additionally, rapid cooling can decrease the perfect crystallization, depending on the specific crystallization kinetics [24].

The manufacturing of the polymer samples can be achieved through a variety of manufacturing methods. The chosen method of elevated temperature extrusion with specific post extrusion operations presents a common polymer forming method already widely used in industry. The optimization efforts preformed during this process allowed for the generation of sample wafers meeting all of the criteria required for the future electrodeposition processes. It is observed further enhancements to the mechanical properties, specifically the ductility, of the polymer can be realized by the addition of the compression or rolling step after the extrusion. Thus these samples that are extruded and rolled are used henceforth as the substrate, upon which the electroplated coatings are analyzed.

Chapter 4

Simulations

The ability to perform simulations in preparation as well as concurrently with experimentation is of great aid to the modern engineer. This chapter covers the two primary simulations completed throughout this analysis. The first models the effect of film porosity as it relates to extrinsic stressing. The second simulates the unique condition wherein instrumented indentation is preformed on a thin film atop a relatively softer substrate. Engineering software packages COMSOL Multiphysics and ANSYS are used for these simulations, respectively. COMSOL is chosen for the extrinsic stress analysis for its powerful numerical capabilities concerning the generation and distribution of a static stress. ANSYS is chosen for the nanoindentation simulations for its dynamics package which allow for the analysis of two members coming into contact with each other, and the resulting displacements and failure mechanics.

4.1   Effect of Porosity on Stress Distribution

Stresses in thin films are an unfortunate reality and are divided into two primary categories; intrinsic and extrinsic. The former represents the internal stresses in the film inherited during the formation process and resulting from a multitude of factors such as; specific growth of grains, impurity incorporation, grain boundary relaxation, moisture interactions, vacancy removal, etc [25]. Extrinsic stresses are those resulting from externally applied changes in environment, after the forming process. Extrinsic stresses may result from environmental changes such as thermal variation (only extrinsic stress inducing if film and substrate do not have same thermal expansion coefficient), or applied loads such as external forces and moments.

This first simulation aims to cover only extrinsic stresses, and how these stresses flow throughout the film. It is observed during the scanning electron microscopy analysis (results presented in Chapter 5) that the various electroplating methods resulted in varying levels of film porosity. With the effects of film

porosity on stress distribution unknown, COMSOL Multiphysics is utilized to examine this phenomenon. It is desirable to minimize stresses in the film and substrate, as local and average stressors can promote debonding of the film (as discussed in Chapter 5)

For the simulation two geometries are generated, common to both simulations is the substrate. For the substrate a 1 mm by 1 mm square with a height of .5 mm is modeled and polyethylene is assigned as the material. Similarly both models have a 10 micron thick metallic film located atop the substrate. For the first model the film remains intact, covering the entire substrate top surface, Figure 4.1. For the second model, the film is mutilated to model porosity in the range of 1 local vacancy per 10,000 square microns of film. The local vacancies are modeled as 5 micron diameter holes passing through the film, Figure 4.2.
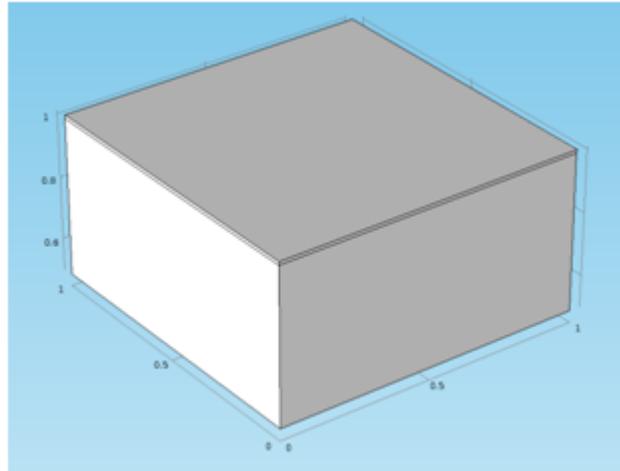
Figure 4.1: Geometric model for non-porous film atop a substrate
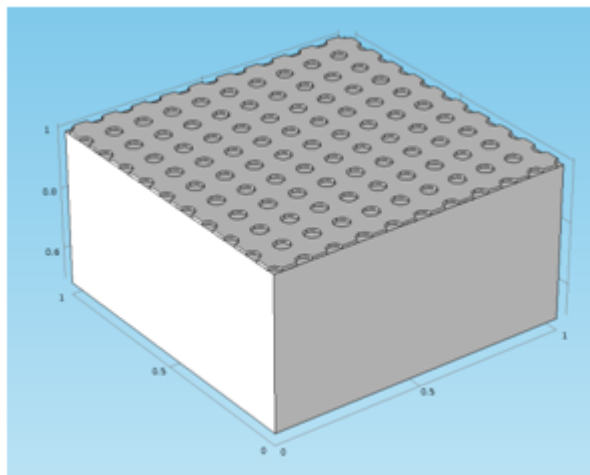
Figure 4.2: Geometric model for porous film atop a substrate

The extrinsic stress is introduced as a body load applied to a vertical side of the substrate. The opposing side represents the boundary condition as a fixed constraint of zero displacement. Cantilever style bending occurs as a result, introducing stress into the film, the film/substrate boundary, as well as the substrate. An appropriate mesh is selected for each geometry and the simulations are run until the convergence criterion is met (initial simulation parameters included a higher refined mesh with a larger surface area to monitor the macroscopic stress effects with greater detail, however, do to computation power limitations the simulation had to be optimized for the compter running the simulations).

The results are presented as von Mises Stress with units of N/m^2. The first model with a continuous film depicts a relatively smooth stress distribution with a maximum stress value of 1.374 N/m^2 at the leading edge of the film at the fixed boundary (while this value has no inherit meaning it will be used for comparative purposes), Figure 4.3. The second model presented in Figure 4.4 depicts the porous film geometry with a similar overall stress distribution transition. Although the vacancy sites result in interruptions of the stress distribution, yielding a maximum stress of 3.467 N/m^2, over two and a half times greater than the continuous film. The value of 2.5 is known as the stress concentration factor.
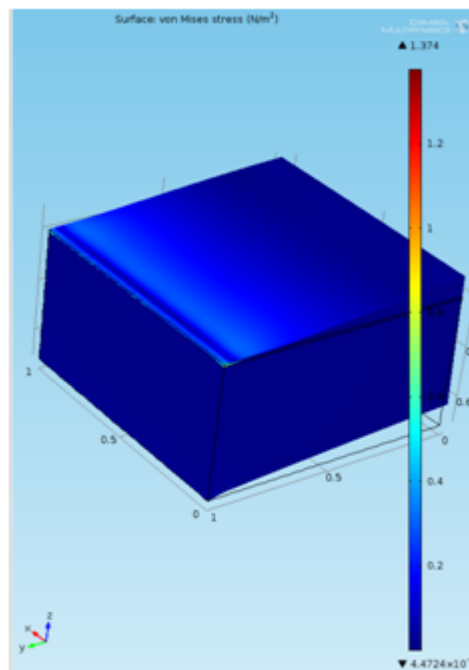
Figure 4.3: Continuous film von Mises stresses for entire body
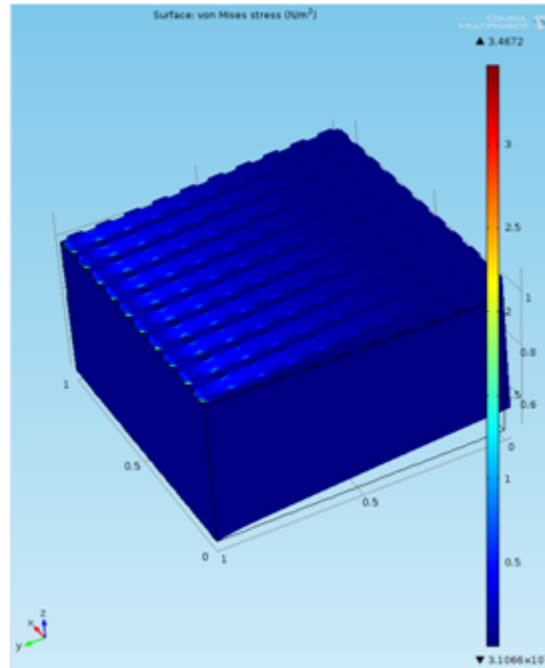
Figure 4.4: Porous film von Mises stresses for entire body

To examine the interactions at the boundary between the film and substrate, cross-sectional views are presented to determine the stress flow from the substrate to the film. Figures 4.5 and 4.6 depict the continuous film model as viewed with cross-sectional slices in the YZ and XZ planes, respectively. It can be noticed the non-linearity in the stress distribution, resulting from the boundary at the film/substrate interface. The stress values are greater in the film, however the values do decrease in a linear fashion as the surface of the film is approached.
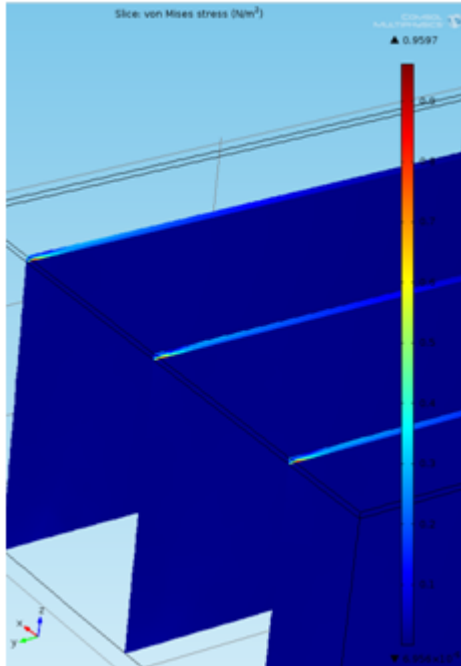
Figure 4.5: Cross sectional view of continuous film model in YZ plane
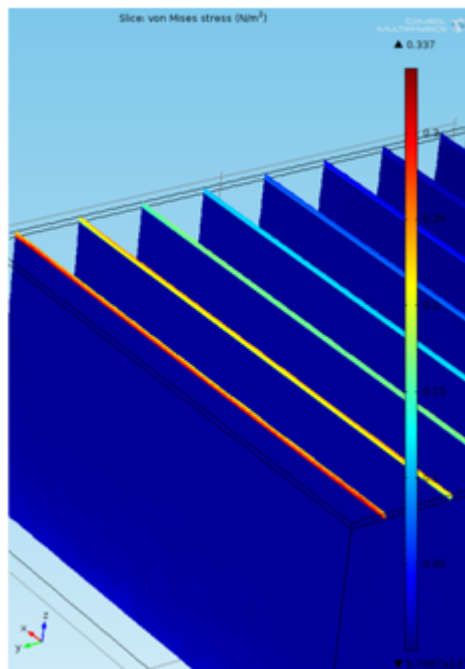
Figure 4.6: Cross sectional view of continuous film model in XZ plane

The equivalent cross-sectional views are also presented for the porous film model, Figures 4.7 and 4.8. A similar discontinuity is noticed at the film/substrate interface; however, beyond the interface the porous geometry dominates the resulting stress distribution. This effect is best represented in Figure 4.8 where

regions of relatively low stress develop in-between adjacent vacancies. Consequently, regions of relatively high stress develop in the areas that do not have vacancies in their plane.
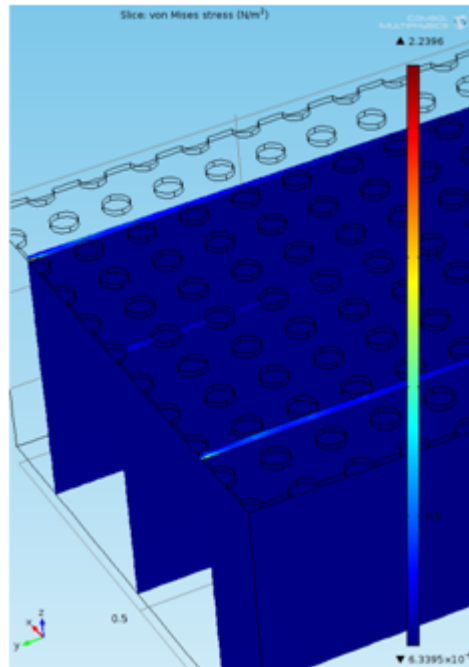
Figure 4.7: Cross sectional view of porous film model in YZ plane
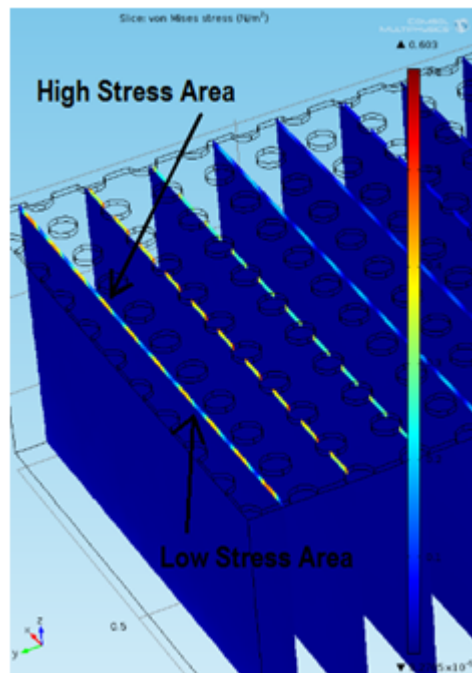
Figure 4.8: Cross sectional view of porous film model in XZ plane

The periodic regions of high and low stress are due to the geometry of the porosity. As the compressive

stress builds in the film, the vacancies deform as they begin to "crush" inwards on themselves. This deformation relieves some of the compressive stress between adjacent vacancies. However, the regions without vacancies then undergo a higher compressive stress, as these regions must carry additional loads to make up for the vacancies in the rest of the film, resulting in larger local stresses for the porous film.

The results of the COMSOL simulations indicate that the relative stress levels of the thin film (represented in the simulations as the upper layer) will increase when relatively small, repeated regions of the film are removed (representing porosity in the deposited film). The discontinuity in the coating allows local stress concentrations to form at the boundaries of the discontinuities. Local stress concentrations often indicate regions first to succumb to failure, thus it is desired to minimize porosity in the film.

4.2   Nanoindentation of Thin Film

Instrumented indentation is preformed on every sample considered in this analysis. Despite various deposition parameters, all samples share the common trait of a metallic film located atop a relatively softer substrate. As deformations can occur in the substrate as well as the film, the primary difficulty presented with this measurement technique is to distinguish the contributions of the film from those of the substrate [20]. Various theories and methodologies are presented in Chapter 2 to relate and separate these effects, with varying levels of certainty and success.

To circumvent this issue it is desired to determine the highest percent depth for a given material at which deformation is limited to the film. To determine this value simulations are preformed using the software ANSYS and the Transient Structural mechanical application. The model consists of an indenter tip, film, and substrate. The geometry of the indenter tip is modeled as non-ideal as experimental data has shown tip geometries deviate from the ideal shape due to wear and the crystallographic structure of the diamond material [26]. Thus the tip is truncated by 10 nm to provide more realistic tip geometry and assigned diamond as the material.

The film is modeled as a 250 micrometer diameter cylinder (which allows for a semi-infinite analysis method in which the stress propagation does not reach the boundaries of the film) with a thickness of 10 microns. The substrate, also modeled as a cylinder, has the same diameter but a thickness of 700 microns. Thus the relationship between the thicknesses of the film and substrate are representative of the actual samples. The material of the film is designated as nickel than as copper such that two simulations are completed modeling both film materials. The substrate is modeled as a modified polyethylene mimicking the mechanical properties of the nanoengineered polymer used in the samples. A symmetry condition is utilized such that only one quarter of the actual model is needed for the simulations, Figure 4.9.
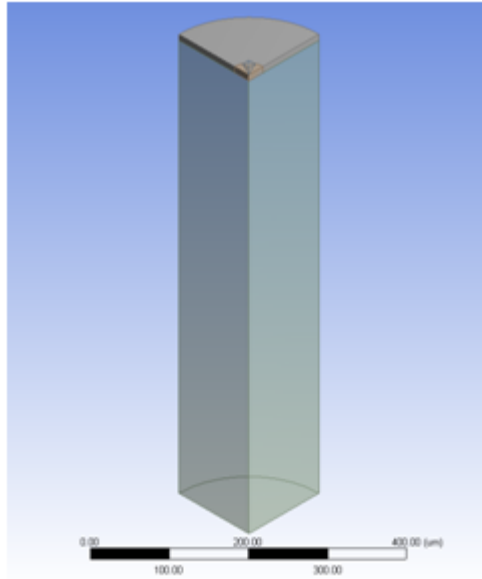
Figure 4.9: Geometry used for the Nanoindentation Simulations

Meshing is performed using the ANSYS solid mechanics package in a manner such that a more refined mesh is generated at the theoretical center of the film and substrate where the interaction of the indenter tip and film will occur. This is accomplished using a MultiZone meshing technique that decreases the relative mesh element size as the center of the film is approached. The meshing of the substrate is also enhanced such that it consists of 75 divisions along the depth of the geometry. Additionally, a section of the film located near the indenter tip is sanctioned such that a more refined mesh can be applied to this area, Figure 4.10.
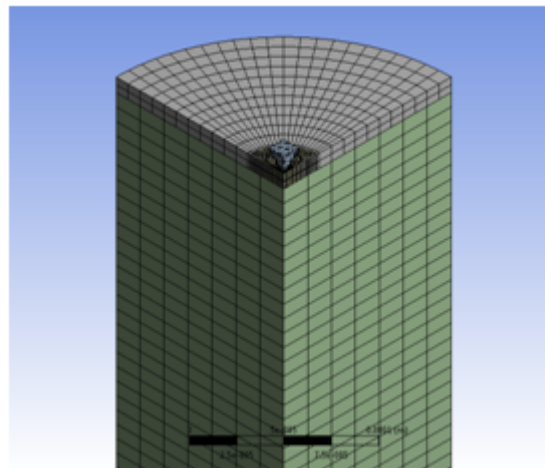
Figure 4.10: Meshed Model of the Geometry used for the Nanoindentation Simulations

Both simulations of the nickel and copper films are completed with the same physics applied. Ini-

tial simulation parameters utilized an explicit dynamics package to model the interaction between the indenter tip and the films. However, due to the relatively slow approach speed of the indenter the explicit dynamics approach failed to recognize a convergence criterion. Thus the simulation package was switched to an implicit dynamics physics model which allowed for a greater in simulation time. Thus the actual speed of the indenter tip was able to be modeled. Namely, a linearly increasing force is applied to the indenter tip in the direction of the film, "B" in Figure 4.11. The magnitude range of the force is selected such that resulting velocity of the indenter tip is representative of the actual instrumented indentation experimental indenter tip velocity (4000 nanometers per minute). Also consistent with the actual experimental indentation is the location of the counter acting force, which is the bottom face of the substrate, "A" in Figure 4.11.
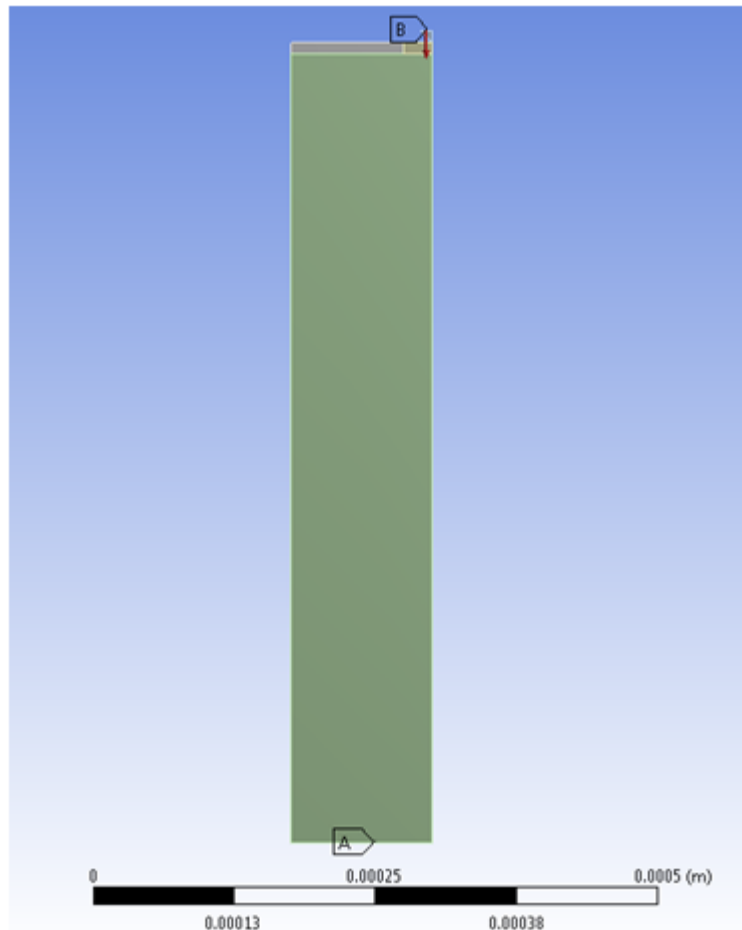
Figure 4.11: Applied Boundary Conditions of the Physics using for the Nanoindentation Simulations

The simulations determine the maximum indenter tip depth before deformation of the substrate is realized. The indenter tip will continue to penetrate into the film (causing a displacement of the film) until displacement of the substrate is encountered, at which time the simulation terminates. Thus the

simulation is prepared and run until this criterion is met; the results presented include the indenter tip depth immediately preceding substrate deformation. Figure 4.12 presents the results for the simulation utilizing a nickel substrate, while Figure 4.13 presents the results for the simulation utilizing a copper substrate.
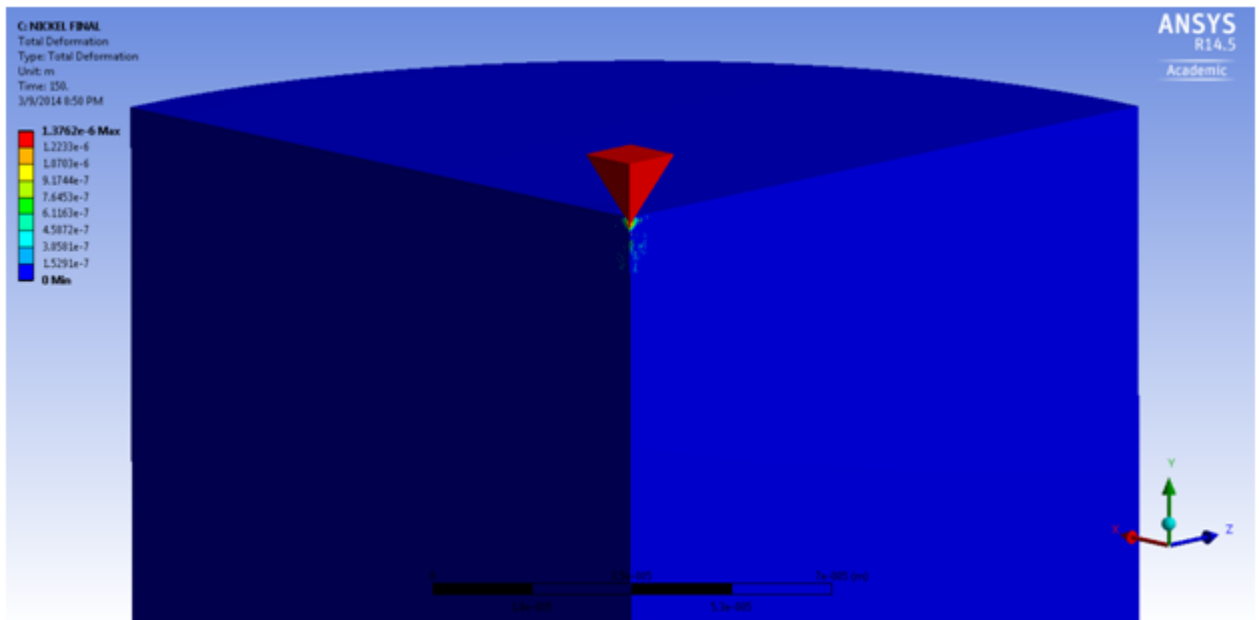
Figure 4.12: Nanoindentation Simulation Results for the Nickel Film case
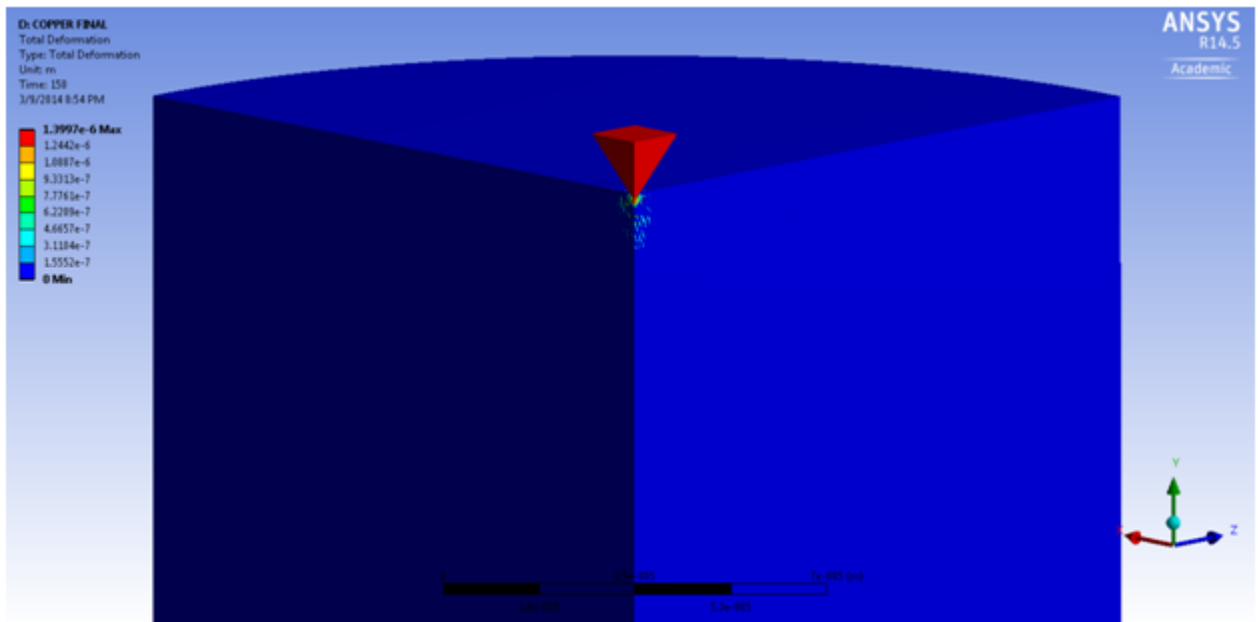
Figure 4.13: Nanoindentation Simulation Results for the Copper Film case

As presented in Figure 4.12 and 4.13, the maximum indenter tip depth that can be achieved before deformation of the substrate occurs is 1.3762 and 1.3997 microns for a nickel and copper film, respectively. As expected the magnitude of the indenter tip depth is greater for the softer copper film in which the film can "absorb" a greater amount of energy resulting in less energy transfer to the substrate that will ultimately cause substrate deformation.

It is desired to select a single value to be used for the actual indenter tip depth for the experimental data acquisition, to ensure consistent data collection parameters across all samples. Thus the results from the nickel film simulation will be solely examined as deformation reaches the substrate first under these conditions (as compared to the copper film simulation). Given the 10 micron thick nickel film the indenter tip was able to reach a maximum depth of 1.3762 microns with deformation contained to the film (no displacement of the substrate). Thus it is theoretically determined that the indenter tip in both cases (nickel film and copper film) may reach a depth approaching 13.76% of the films total thickness, without introducing effects from the substrate. This result is consistent with the work completed by Sakharova et al who stated (depending on the ratio of the film hardness to composite hardness) that for a composite when the indentation depth approaches 1/10 of the film thickness, the substrate almost does not contribute to the measured hardness [20].

Chapter 5 presents the data collected during the deposition procedure for all the samples. Included in this data is the theoretical thickness of every film. Again to ensure consistent data collection parameters

across all samples the minimum thickness film will be used as the control. As presented in Table 5.8 the minimum calculated thickness occurs for Sample N1, at 8.35 microns. Using the results from the simulations, 13.76% depth is calculated for the 8.35 micron thickness. The calculation of which results in a maximum indentation depth, without substrate deformation, across all samples of 1.149 microns. To provide for a margin of error the set value for the indenter tip depth is selected as 1 micron, or 1000 nm, for all instrumented indentation data collection.

Chapter 5

Electroplating of Metallic (Ni & Cu) Films and Characterization

This chapter provides the details of the results of our studies on electroplating of Nickel and Copper films on the prefabricated nanoengineered polymer substrate. It also includes the results and analysis of the electroplated films and correlation of it properties to the plating conditions. In pulse electroplating, some of the most important parameters were analyzed. These are Duty Cycle, Current Density, and plating duration. These are further discussed below.

5.1 Duty Cycle

There are numerous factors that alter the deposition and properties of an electroplated material. This research aims to focus on the four largest factors with the goal of optimization a given set of parameters. Optimization is defined in this context as an electroplated coating with superior mechanical and electrical properties. The first factor considered is the duty cycle at which the electroplating operation is preformed at. The equation for which is presented below, Equation 5.1. Perhaps the most common duty cycle results from 100%, known as Direct Current (DC) plating. In DC plating, there is no interruption of the current flow to the cathode/anode.

$$DutyCycle = \frac{Time_{ON}}{Time_{ON} + Time_{OFF}}$$ (5.1)

Pulse plating covers the range of duty cycles from greater than 0% to less than 100%. The result is a periodic interruption of current flow. This interruption allows for a dispersion of a negatively charged layer that forms around the cathode while current is applied. This layer can inhibit ion mobility, thus

decreasing the process efficiency [27]. Early work by W. Kleinekathofer indicated pulse plating (as compared to DC) has a finer microstructure and a reduced porosity [28]. Although it is further stated in the article that the "...properties of pulse plated nickel are affected by too many factors in order to make a general statement." [28].

One effect of the usage of pulse plating is the requirement of a higher peak current to maintain a constant cathode current density, as described by Equation 5.2. For low duty cycles this can produce a large spike in the current, which can lead to "burning" of the deposited material. Burning is a term used to describe the adverse effects on a plated deposit caused by a sufficiently large ratio of applied current to the limiting current (limiting current determined by the availability of ions in the electrolyte) [29].

For example if a 100 mA average current is desired with a 10% duty cycle operating at 1 Hz; the result would be a 1 Amp current flow for .1 seconds followed by a .9 second pause with no current flow.

$$Current_{AVERAGE} = Current_{PEAK} * Duty\ Cycle \tag{5.2}$$

5.2   Current Density

The flow of current from the power supply is directly proportional to the current density. Current density is the ratio of applied current to the area to be plated. The units mA/cm^2 will be solely used throughout this analysis in reference to current density. The primary effect of current density is the rate at which the material is deposited onto the cathode. Thus for a higher current density, a given amount of deposit is achieved in a shorter period of time. The increase in current density is brought on by an increase in the average current (given a constant plating area). This can result in adverse effects on the microstructure of the deposited material, as discussed in Chapter 2.

5.3   Duration

The sole effect of the duration of plating is the accumulation of the deposited material. This relationship is ideally linear, given steady state conditions of the electroplating bath (no changes in temperature, composition, pH, etc). The amount of deposited material linearly increases the thickness of the coating (given a constant plating area). A minimum amount of deposited material is required to ensure film continuity and thus electrical conductivity across the plated area. However, as thickness is increased, internal stresses in the deposit also increase [30]. Stresses in the metallic film result in poor adhesion as stresses promote debonding [30]. The thickness of the film is regarded as a performance indice as it relates to stresses and adhesion.

Alternatively Freund and Suresh present a notion that average stress is a product of the thickness of the film and can vary between compression and tension in a single deposition [25]. Based on the work completed by Floro et al. it was observed the average stress begins compressive then migrates to an average tensile stress, and lastly plateaus as a compressive stress, Figure 5.1. This phenomena was observed for several film and substrate combinations at various deposition temperatures.
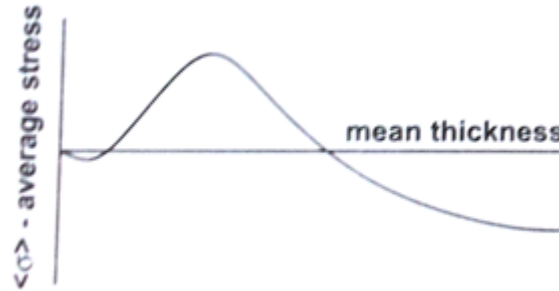
Figure 5.1: Average stress as a function of the deposited film thickness [25]

The basis of this analysis centers on the manipulation of these variables and how they influence the primary optimization of parameters. The optimization parameters include two principal targets, low resistance of the film, and superior adhesion. These goals also encompass secondary components, in the case of adhesion, stresses between the film and substrate can promote debonding [30]. Other factors influencing the adhesion include the mechanical properties of the film and substrate, such as; Young's Modulus, hardness, and the surface roughness of the films [31].

5.4 Electroplating of Nickel and Copper

A systematic study is undertaken by plating 24 samples which are analyzed for different properties. These samples cover the range of parameters discussed in earlier sections in this chapter, using the substrates identified in Chapter 3. The samples are generated in random order (within each material designation) to eliminate any time dependant factors that may skew the analytical results. A special electroplating jig is designed and fabricated for electroplating of these samples.

As it is desired to deposit a film on only one side of the substrate, a unique fixture is designed that allows for complete submergence of the sample, while only presenting one side of the sample to the electrolyte solution. Figure 5.2 presents the CAD drawing of the fixture, Figure 5.3 presents the actual fixture machined from Teflon at Western Michigan University. Teflon is chosen as the material due to its electrically insulatory property as well as its inert tendency to any aggressive electrolyte solution.
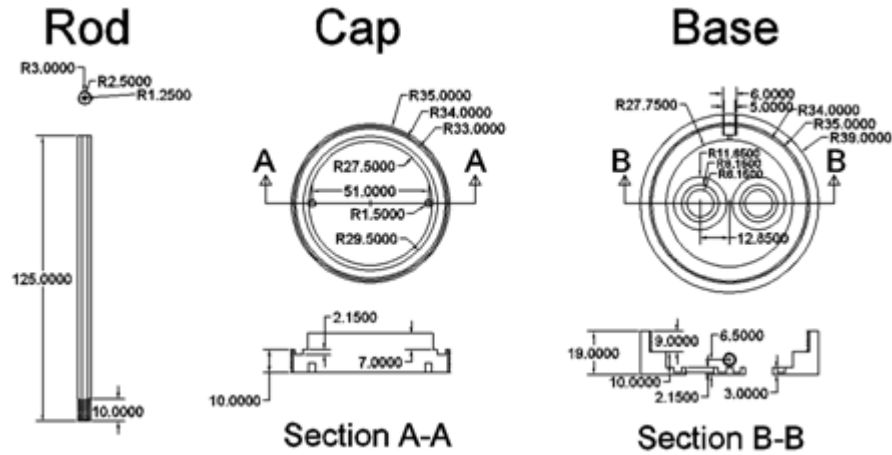
Figure 5.2: Design of Plating Fixture

Figure 5.3: Fixture used for Electroplating

The chosen electrolyte solution is taken in a 1000 mL Pyrex beaker and placed on a hot plate, Figure 5.4, to maintain the electrolyte temperature at the required volume. The electrolyte temperature is continuously monitored by a thermometer. Also presented in the figure is the anode (nickel plate in the figure), as well as the sample fixture. Figure 5.5 presents the current source used for the experimentation, a Dynatronix MicroStar Pulse Precise Series DuPR10-.5-1.5XR Pulse Power Supply, capable of providing 1.5 A peak current (.5 A continuous) at a maximum of 10 volt output, with a 1 mA increment resolution.
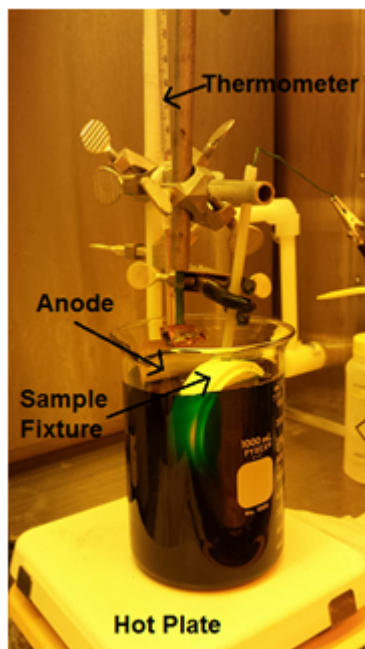
Figure 5.4: Electroplating Bath

Figure 5.5: Dynatronix DuPR10-.5-1.5XR Pulse Power Supply

In these experiments two parameters are varied, the duty cycle (25%, 50%, 75%, and 100%) and current density (5 mA/cm^2, 10 mA/cm^2, and $15mA/cm^2$) and their effect on the resulting films properties was studied in a systematic way. The material to be deposited (copper and nickel) was also examined. The electrodeposition time is held constant at 60 minutes per sample, as deposition time dependant intrinsic stress analysis is outside the scope of this research. Thus the design of experiments table based

on these parameters is presented in Table 5.1 and 5.2.   Preceding the deposition process the power

Table 5.1: Design of Experiments Table for Nickel with Sample IDs

Current Density/Duty Cycle	25%	50%	75%	100%
5 mA/cm$\hat{2}$	N1	N2	N3	N4
10 mA/cm$\hat{2}$	N5	N6	N7	N8
15 mA/cm$\hat{2}$	N9	N10	N11	N12

Table 5.2: Design of Experiments Table for Copper with Sample IDs

Current Density/Duty Cycle	25%	50%	75%	100%
5 mA/cm$\hat{2}$	C1	C2	C3	C4
10 mA/cm$\hat{2}$	C5	C6	C7	C8
15 mA/cm$\hat{2}$	C9	C10	C11	C12

supply is adjusted to the designated duty cycle and current density. The current density is based on the area of the sample to be plated which includes two, 1.85 cm diameter circles, with a total plated area of 5.376 cm^2. The duty cycle is programmed to have a period of 20 ms, 50 Hz (with the exception of the 100% duty cycle, where frequency is not applicable). Given the area to be plated and the desired frequency, Table 5.3 and 5.4 presents a summary of the programmed power supply parameters for these samples. For each sample, numerous statistics are recorded prior, during, and post electrodeposition to

Table 5.3: Summary of Power Supply Parameters

Sample ID	Current Density (mA/cm$\hat{2}$)	Average Current (mA)	Max Current (mA)
N1 / C1	5	26.88	107.52
N2 / C2	5	26.88	53.76
N3 / C3	5	26.88	35.84
N4 / C4	5	26.88	26.88
N5 / C5	10	53.76	215.04
N6 / C6	10	53.76	107.52
N7 / C7	10	53.76	71.68
N8 / C8	10	53.76	53.76
N9 / C9	15	80.64	322.56
N10 / C10	15	80.64	161.28
N11 / C11	15	80.64	107.52
N12/ C12	15	80.64	80.64

document key deposition conditions and results. Prior to the deposition each sample's mass is recorded, and once the deposition has begun the electrolyte's pH is also documented, Table 5.5 and 5.6. It may be observed from Table 5.5, that efforts were made to keep the electrolyte solution pH to be constant. In cases where the pH has changed dramatically, a fresh plating solution is prepared to ensure similar plating conditions for all samples. At the start of the deposition the power supplies applied voltage is recorded (a function of the applied current and the resistance between the electrodes), as well as at the

Table 5.4: Summary of Power Supply Parameters, cont

Sample ID	Time On (ms)	Time Off (ms)	Duty Cycle
N1 / C1	5	15	25%
N2 / C2	10	10	50%
N3 / C3	15	5	75%
N4 / C4	N/A	N/A	100%
N5 / C5	5	15	25%
N6 / C6	10	10	50%
N7 / C7	15	5	75%
N8 / C8	N/A	N/A	100%
N9 / C9	5	15	25%
N10 / C10	10	10	50%
N11 / C11	15	5	75%
N12/ C12	N/A	N/A	100%

end of the deposition. The applied voltage consistently drops during the electroplating process as the resistance between the electrodes decreases due to the addition of the metallic film on the surface of the substrate. This decrease in voltage is assumed to be linear and as such the two values are averaged for analytical purposes in calculating the average resistance between the cathode and anode, Table 5.5 and 5.6.

Also during the deposition process the actually current supplied to the electrodes is recorded. While this value would ideally stay consistent to the set value, mechanical limitations introduce deviations, especially for the lower duty cycle samples. This is due to the inability of the power supply to provide instantaneous current from an OFF setting. These deviations are recorded and used to calculate the actual current density, presented in Table 5.6. At the conclusion of the electroplating process the sample is removed from the fixture and once again the mass is recorded (at a sufficiently later time as to ensure any residual moisture has evaporated). Subtracting this value from the previously measured mass allows for the determination of the film's mass. Using the expected density of the plated film's material ($8908 \ kg/m^3$ for nickel and $8940 \ kg/m^3$ for copper) [32], and the area of the plating, the theoretical film thickness can then be calculated, Table 5.7 and 5.8. Also presented in Table 5.8 is a measure of the film's resistance after completion of plating. The current efficiency is documented for each sample, as calculated by the equation in Chapter 2.1. As presented in the table, it may be seen that the current efficiencies of the electroplating process while plating Nickel as well as Copper is above 90%, which clearly indicates that the majority of the current applied is well utilized for the plating process alone.

An important consideration regarding the collected data during the deposition process is the actual average current provided by the power supply. It is noticed that in some instances (particularly the lower duty cycle, higher current density combinations) the actual average current deviates from the ideal by a significant amount. This can be due to an insufficient power supply which cannot provide sufficient

Table 5.5: Summary of Data Recorded During the Electrodeposition Process

Sample ID	Electrolyte pH	Starting Voltage (V)	Final Voltage (V)	Average Voltage (V)
N1	3.2	2.49	2.52	2.51
N2	3.7	4.08	3.93	4.01
N3	3.59	5.52	4.99	5.26
N4	3.28	4.83	4.26	4.55
N5	3.3	2.5	2.5	2.5
N6	3.42	5.02	4.98	5
N7	3.61	7.53	7.55	7.54
N8	3.4	7.4	6.06	6.73
N9	3.62	2.5	2.5	2.5
N10	3.28	5.01	5.01	5.01
N11	3.38	7.52	7.48	7.5
N12	3.49	9.99	9.99	9.99
C1	0.37	2.51	2.52	2.52
C2	0.42	2.8	2.52	2.66
C3	0.41	3.38	2.95	3.17
C4	0.35	3.51	2.92	3.22
C5	0.4	2.52	1.35	1.94
C6	0.41	5	4.98	4.99
C7	0.43	5.4	5.05	5.23
C8	0.4	5.58	5.24	5.41
C9	0.4	2.5	2.5	2.5
C10	0.4	5.01	5.03	5.02
C11	0.45	7.51	7.51	7.51
C12	0.35	9.99	3.56	6.78

current switching. As such the actual current density deviates from the ideal which will have implications for the electrodeposited films. This can be a significant source of error concerning the characterization of the electroplated films. Optical microscope pictures of the nickel samples are presented in Figure 5.6, while that of copper samples are presented in Figure 5.7. It is noticed from these images some leaking occurs past the o-ring seals and allows for undesired deposition on areas other than the designated circles. Additionally, voids appear near the top of many samples as a result of air entrapment against the edges of the o-ring seals. These discrepancies result in a change in the plating area that is not accounted for in the analysis. As such this can be a source of error concerning the results assuming a constant, consistent plating area.

Table 5.6: Summary of Data Recorded During the Electrodeposition Process, cont

Sample ID	Actual Current (mA)	Actual Current Density (mA/cm^2)
N1	19.7	3.66
N2	26.9	5
N3	26.8	4.99
N4	26.9	5
N5	24	4.46
N6	52	9.67
N7	36.6	6.81
N8	53.8	10.01
N9	24	4.46
N10	32	5.95
N11	79	14.69
N12	67.5	12.56
C1	19.9	3.7
C2	26.9	5
C3	26.8	4.99
C4	26.9	5
C5	54	10.04
C6	53.4	9.93
C7	53.8	10.01
C8	53.8	10.01
C9	38	7.07
C10	47	8.74
C11	71.2	13.24
C12	80.6	14.99

Figure 5.6: Photographs of the Nickel Samples

Table 5.7: Summary of Data Recorded Following the Completion of the Electrodeposition Process

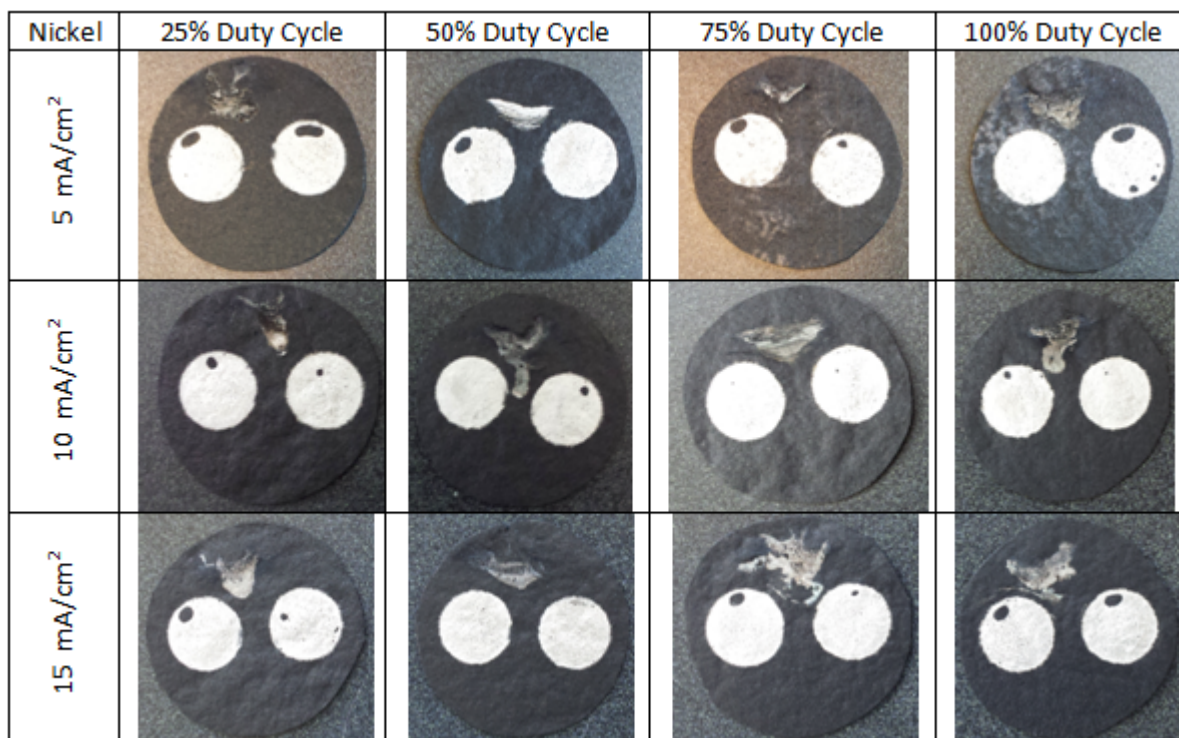| Sample ID	Substrate Mass (mg)	Substrate and Film Mass (mg)	Film Mass (mg)
N1	1819	1839	20
N2	1761	1788	27
N3	1910	1937	27
N4	1839	1871	32
N5	1874	1898	24
N6	1926	1978	52
N7	1855	1892	37
N8	1842	1892	50
N9	1857	1882	25
N10	1905	1939	34
N11	1892	1973	81
N12	1912	1979	67
C1	1953	1976	23
C2	1918	1949	31
C3	1926	1957	31
C4	1879	1911	32
C5	1844	1902	58
C6	1844	1903	59
C7	1950	2012	62
C8	1861	1922	61
C9	1916	1955	39
C10	1894	1947	53
C11	1857	1936	79
C12	1799	1887	88

Figure 5.7: Photographs of the Copper Samples

Table 5.8: Summary of Data Recorded Following the Completion of the Electrodeposition Process, cont

Sample ID	Calculated Thickness (*microns*)	Film Resistance (*ohms*)	Current Efficiency (%)
N1	8.35	0.2	92.71%
N2	11.28	0.2	91.66%
N3	11.28	0.2	92.00%
N4	13.36	0.2	100.00%
N5	10.02	0.2	91.32%
N6	21.72	0.2	91.32%
N7	15.45	0.2	92.31%
N8	20.88	0.2	84.87%
N9	10.44	0.2	95.12%
N10	14.2	0.2	97.02%
N11	33.83	0.2	93.63%
N12	27.98	0.2	90.64%
C1	9.57	0.2	97.48%
C2	12.9	0.2	97.20%
C3	12.9	0.2	97.56%
C4	13.32	0.2	100.00%
C5	24.14	0.2	90.59%
C6	24.55	0.2	93.19%
C7	25.8	0.2	97.20%
C8	25.38	0.2	95.63%
C9	16.23	0.2	86.57%
C10	22.05	0.2	95.11%
C11	32.87	0.2	93.59%
C12	36.62	0.2	92.09%

5.5   Characterization

This section presents the resultsof our analysis of the electroplated films, with respect to the current density and duty cycle, for both Nickel and Copper films. A Scanning Electron Microscope (SEM) with Energy Dispersive X-Ray Spectrometer (EDS) attachment is used to study the relative porosity and grain size of the deposits as well as composition with respect to the plating parameters. The results from the instrumented indentation are further presented through a comprehensive Analysis of Variance (ANOVA) statistical analysis.

5.6   SEM and EDS

SEM is an important tool for examining the microstructure of materials, as it allows for direct imaging at high magnification levels. The SEM system utilized in this analysis is a Philips XL30-FEG coupled with an EDAX EDS system. This configuration presents a versatile system with a maximum resolution of 3.5 nm at its maximum voltage of 30 kV. The results derived from this analysis are critical in determination of the optimal parameters for electroplating of a nanoengineered polymer.

To begin SEM imaging the sample must first be loaded onto the stage (shown in Figure 5.8), which is then slid into the vacuum chamber. Using the computer controls the vacuum pump is turned on after obtaining the required vacuum (1*E-5 torr) and the electron beam is activated. Before images can be collected the sample must be focused in the beam detector manually, which also sets the working distance to the sample surface. From this point the magnification level is set and the choice of acceleration voltage and spot size can be selected depending on the specific image being collected.
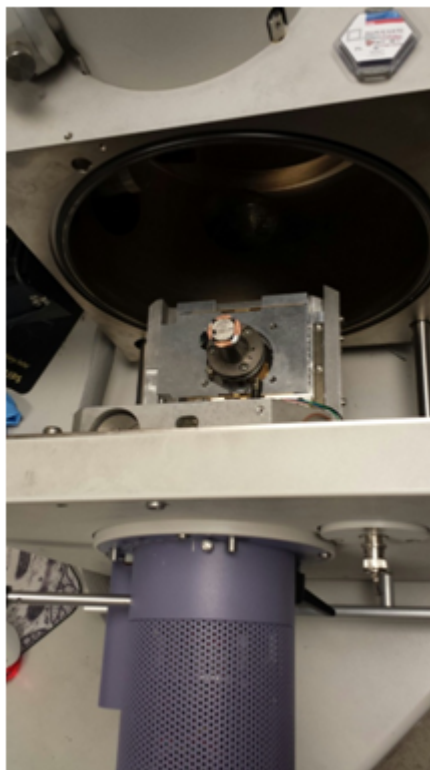
Figure 5.8: Sample loaded onto Stage, Ready to be slid into Vacuum Chamber

The first images collected are at a relatively low magnification (50X magnification) to compare relative porosity levels among the samples with varying duty cycle for Nickel and Copper samples. To provide for an accurate comparison the current density is kept constant, using the samples generated at 10 mA/cm^2. Figure 5.9 presents the images of electroplated Copper and Nickel samples electroplated at different duty cycles from 25% to 100%.

Duty Cycle / Material	Copper	Nickel
25 %		
50 %		
75 %		
100 %		
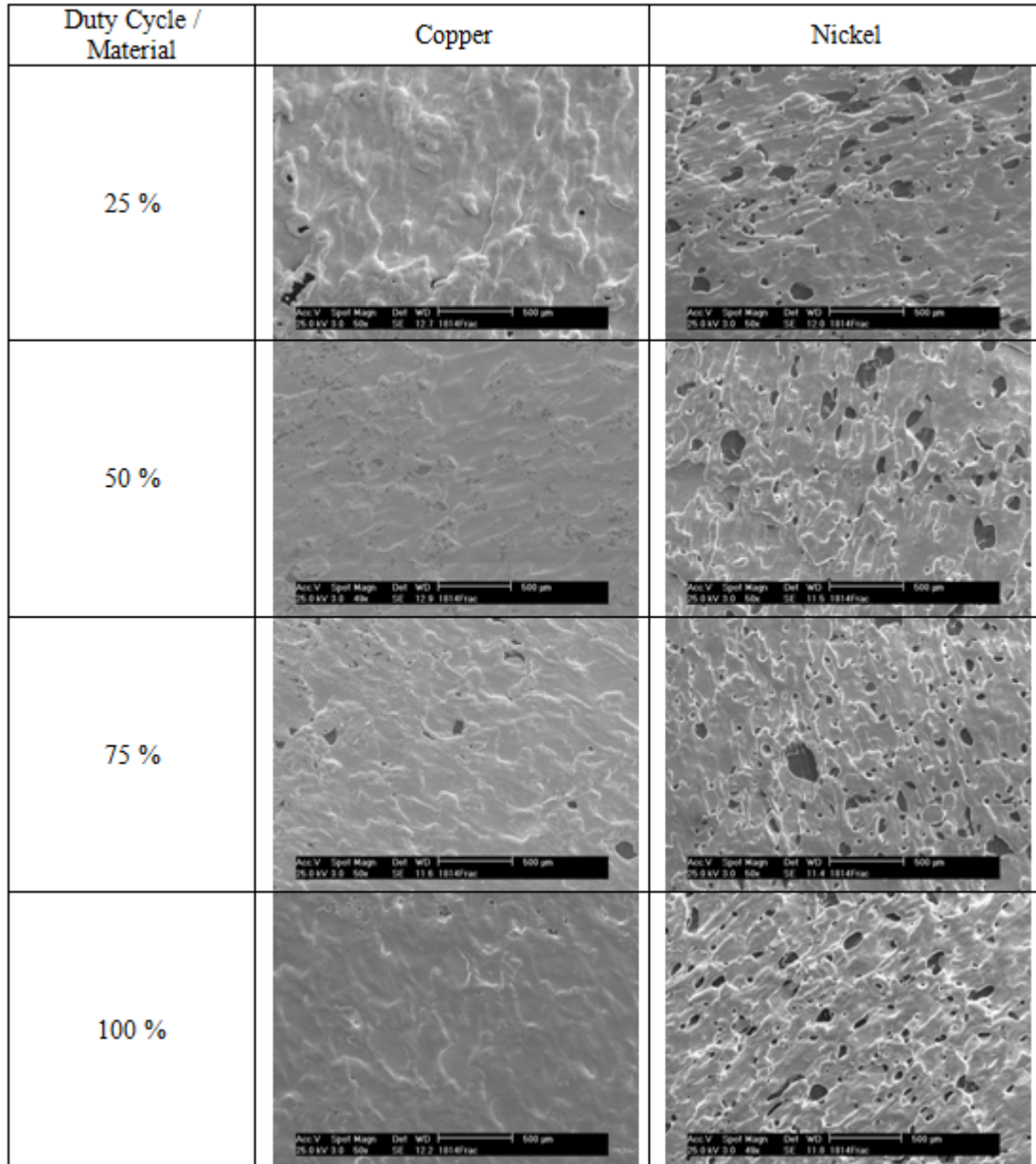
Figure 5.9: SEM Images of Copper and Nickel films depositied at duty cycles 25%, 50%, 75%, and 100%, respectively (50X)

From the SEM images presented in Figure 5.9 it is determined the relative amounts of porosity vary greatly between the copper and nickel deposits. Throughout every duty cycle the copper film presents a greater level of homogeneity with fewer discrepancies. It can also be observed the general trend toward homogeneity of the deposit for samples with increasing duty cycle. This phenomenon can be detected for both the nickel and copper films at different levels. In contrast to Copper films, Nickel has a higher level ofporosity at all duty cycles. The size of the pores was clearly larger at 25% duty cycle compared to the higher values.

Energy Dispersive X-Ray Spectrometry is utilized in the determination of the constituent elements present in the film as well as the voids observed in the film. This characterization of material composition is an important consideration in identifying contamination of the film, salt deposits, incorrect electrolyte bath composition, etc. Two samples are chosen for this analysis electroplated under equivalent conditions (100% Duty Cycle and 10 mA/cm^2) for Copper and Nickel samples, respectively. The EDS spectrum emission collection is completed using identical parameters, namely 25 kV electron beam excitation and a magnification level of $250X$. Figure 5.10 presents the SEM image of the area analyzed for the copper sample.
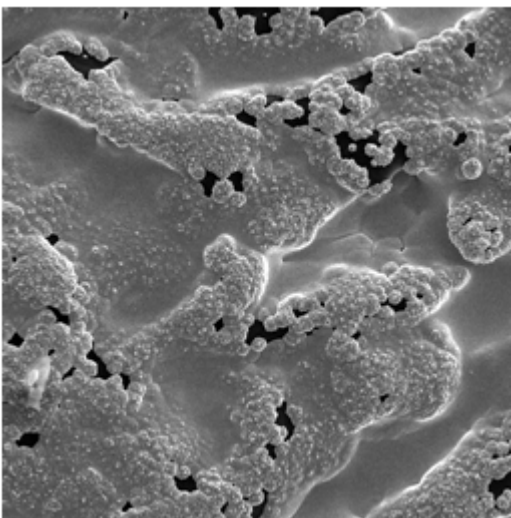
Figure 5.10: SEM Imagine of Area Analyzed during EDS Analysis of the Copper Sample

The EDS analysis automatically analyzes and presents the most prevalent elements within the viewable range. In the case of the copper sample only two elements are recognized, Copper and Carbon. The results of the EDS analysis are presented as maps displaying the relative composition intensity of that specific element. EDS imaging map of Copper films (SEM picture of the same sample shown in Figure 5.10) is presented in Figure 5.11.
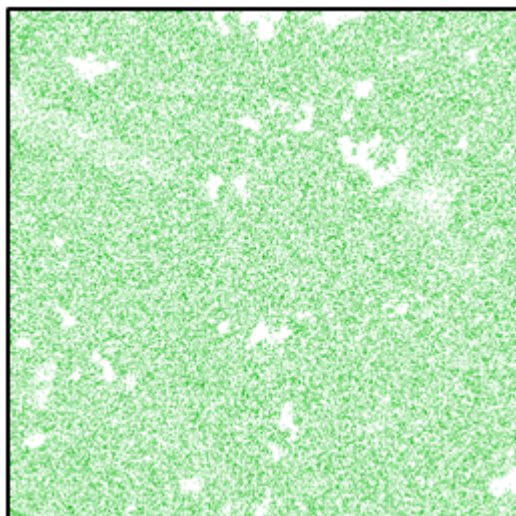
Figure 5.11: EDS Map of Copper for the Copper Film Sample

As expected the composition of the sample is dominated by thepresence of copper (represented by the green area). However white areas are noticed that indicate the lack of copper in various regions. These areas correspond to the aforementioned discrepancies and confirm the previous theory that these are in fact areas where copper deposition has not occurred, and can be correctly referred to as voids. In fact these areas exactly correspond to void areas that can be identified in Figure 5.10. On the macro scale these voids are the constituent discrepancies that determine the relative porosity of the deposited film. The second map generated is that for the element Carbon shown in Figure 5.12. From the Figure it is determined that primarily Carbon is located within the areas earlier referred to as voids. This may be attributed to the Carbon content of the substrate itself.
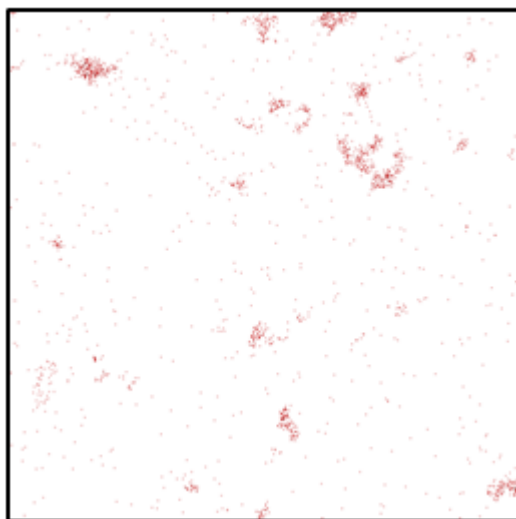
Figure 5.12: EDS Map of Carbon for the Copper Film Sample

EDS imaging is also completed for the nickel sample. Again the EDS analysis automatically analyzes and presents the most prevalent elements within the viewable range, Figure 5.13. In the case of the nickel sample, once again only two elements are recognized, Nickel and Carbon.
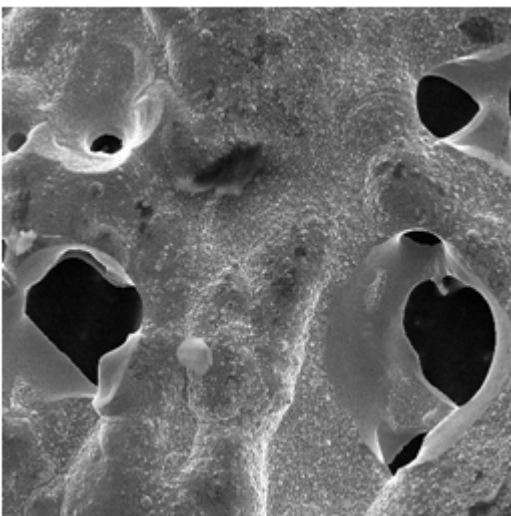
Figure 5.13: SEM Imagine of Area Analyzed during EDS Analysis of the Nickel Sample

Figure 5.14 is the EDS mapping of the element Nickel. Similar to the results for the copper sample, nickel is seen all over the surface of the film. Again the voids are indicated by the lack of presence of nickel. Figure 5.15 presents the EDS map of Carbon which is primarily detected in void areas.
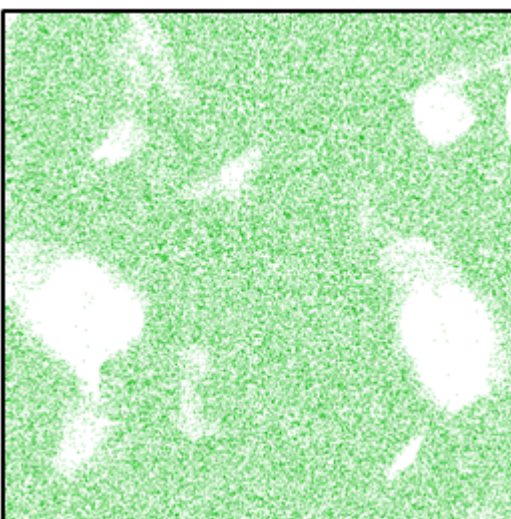
Figure 5.14: EDS Map of Nickel for the Nickel Film Sample
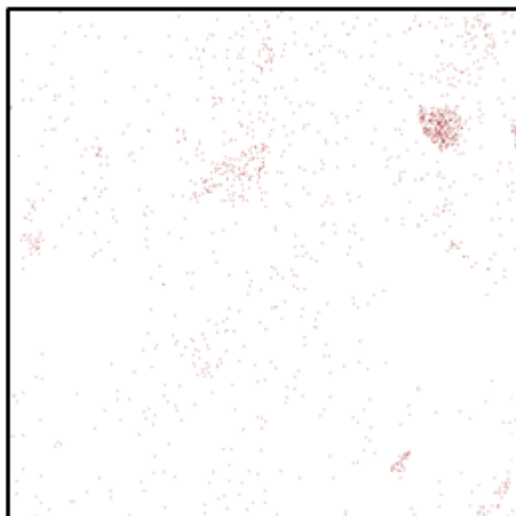
Figure 5.15: EDS Map of Carbon for the Nickel Film Sample

The results of the EDS analysis indicate a successful electroplating deposition with no detectable contamination of the deposited films. As the only other element to be detected by the EDS system was Carbon, which is to be expected. These results also confirm that these electroplated Nickel and Copper films show porosity, at varying levels for Nickel and Copper as shown earlier in Figure 5.9.

In addition to the film porosity, the size of the individual grains that make up the deposited film can also be determined from SEM analysis. Grain size is an important aspect that can affect many physical and mechanical properties. Smaller grain sizes yield significant advantages in terms of wear resistance [33]. Additionally the decrease in grain size leads to an increase in the density of grain boundaries which in turn improves the fracture mechanics of the material. Figure 5.16 presents the samples from Figure 5.9 at a magnification level of $5000X$.

Duty Cycle / Material	Copper	Nickel
25 %		
50 %		
75 %		
100 %		
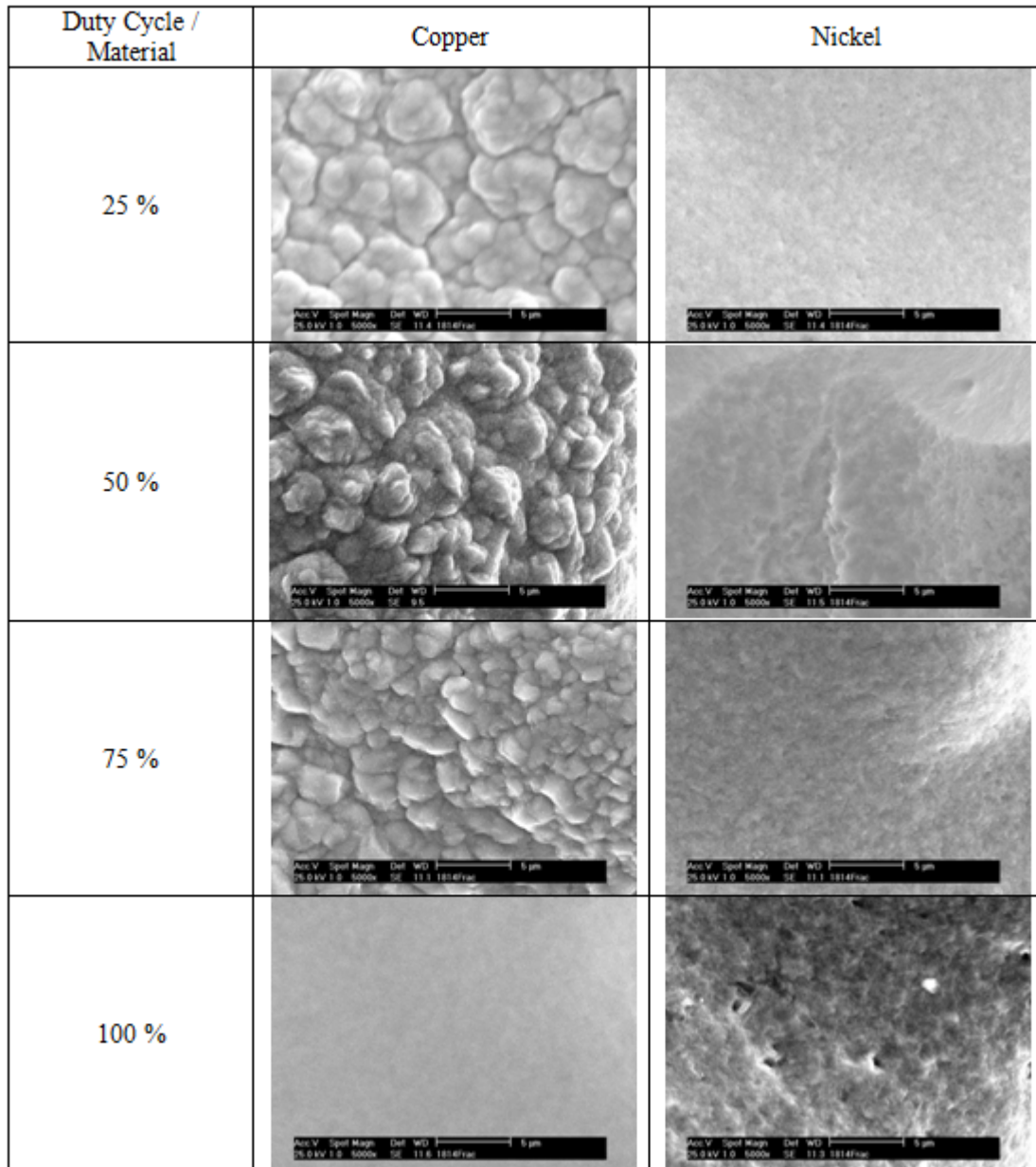
Figure 5.16: SEM Images of Copper and Nickel films depositied at duty cycles 25%, 50%, 75%, and 100%, respectively (5000X)

There is a large amount of variation in the grain size between the copper and nickel films. The grain boundaries can be easily observed for the copper samples, the nickel film however does not exhibit a similar behavior. At a current density of 10 mA/cm^2 and 25% duty cycle the copper film displays a grain size diameter on the order of 2 to 5 microns. Whereas the equivalent nickel sample has too fine a grain structure to be observed at this magnification level. In contrast to Copper films, Nickel films are quite smooth and reflective. Imaging of the samples deposited at a duty cycle of 50% result in an

55

apparent decrease of the copper grain size diameter to approximately 1 to 3 microns, while there is no observable change to the nickel film grain determination. At a duty cycle of 75% the trend continues for the copper film as the grain size diameter is in the range of .5 to 2 microns. The nickel film grain size continues to be indistinguishable at this magnification level.

Switching from the pulse deposited samples (25%, 50%, and 75% duty cycles) to the DC constant current plated samples (100% duty cycle), an interesting phenomenon is observed. While the nickel film grain size is still too fine to be observed, the copper film grain size has decreased to a level that does not allow for its determination. Increasing the duty cycle to 100%, such that no interruptions of the current delivery during deposition occur, has significantly reduced the grain size in the copper film (it is possible this trend also applies to the nickel film although without direct imaging of the grain boundaries it cannot be confirmed).

5.7   Nucleation and Film Growth Study for Nickel

To better understand the nature of the grains comprising the nickel film, it is desired to image the nucleation process and the development of grain structures. To accomplish this nickel plating is preformed at a current density of 10 mA/cm^2 and 100% duty cycle (DC deposition), while subjecting the samples to various deposition times. First examined is the sample with the shortest deposition time studied, five seconds, Figure 5.17.
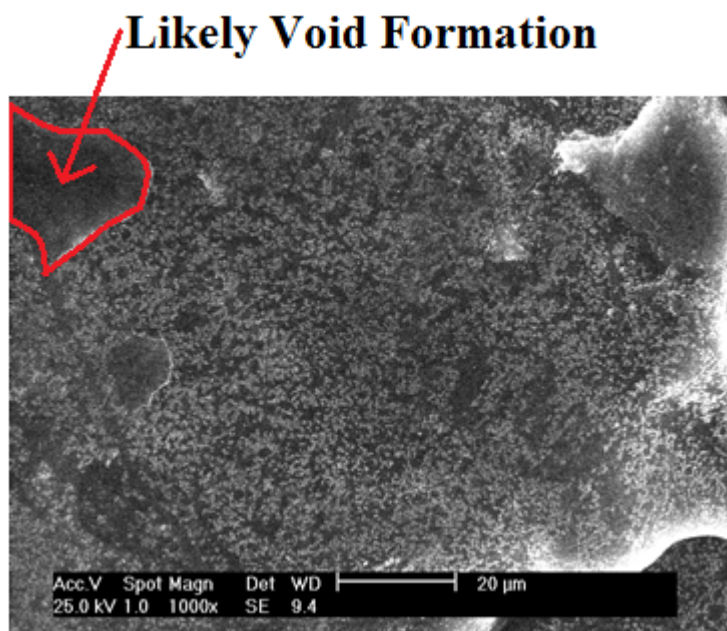
Figure 5.17: Nucleation of Nickel Deposits at $1000X$ Magnification (5 Second Deposition)

From Figure 5.17 the initial stages of the deposition process can be viewed. After just five seconds of current delivery the nucleation of nickel deposits can be observed. This is the first stage in the formation of a thin film. These round sites approximately 250 nm diameter, Figure 5.17, form across the substrate surface. Also from this figure the isolation of certain areas can be viewed, these areas which are inhibiting deposition are likely to result in voids.
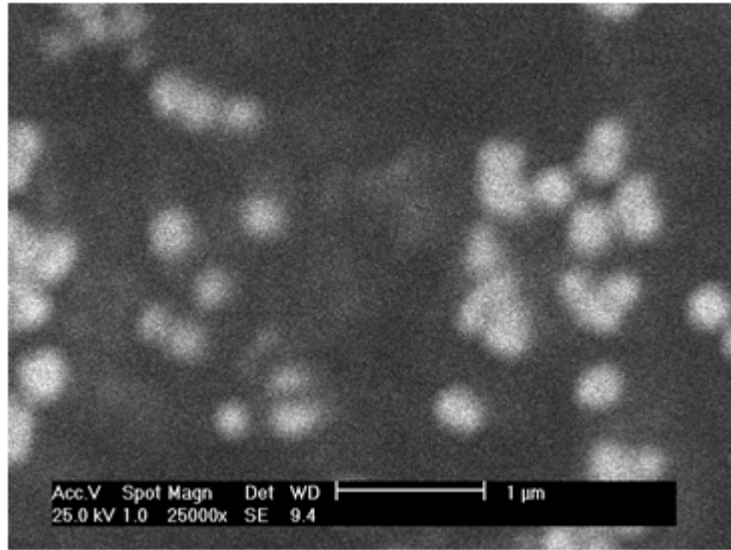
Figure 5.18: Nucleation of Nickel Deposits at $25000X$ Magnification (5 Second Deposition)

The next sample results from a deposition time of 60 seconds. Figure 5.19 depicts the continued growth across the surface of the substrate. After 60 seconds the individual deposits have increased in size to from 250 nm to roughly 1000 nm, Figure 5.20. At $5000X$ magnification it can be seen how the individual grain structures are beginning to form from their nucleation sites, as they begin to intercept other growing grains.
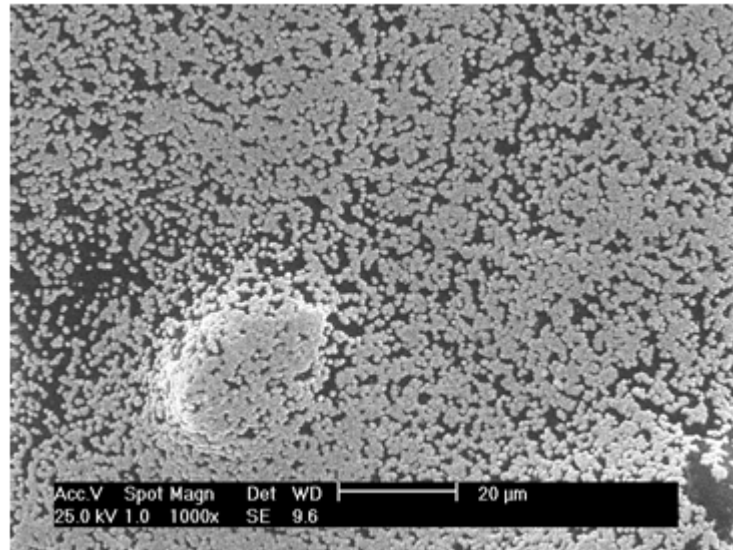
Figure 5.19: Development of Nickel Deposits at $1000X$ Magnification (60 Second Deposition)
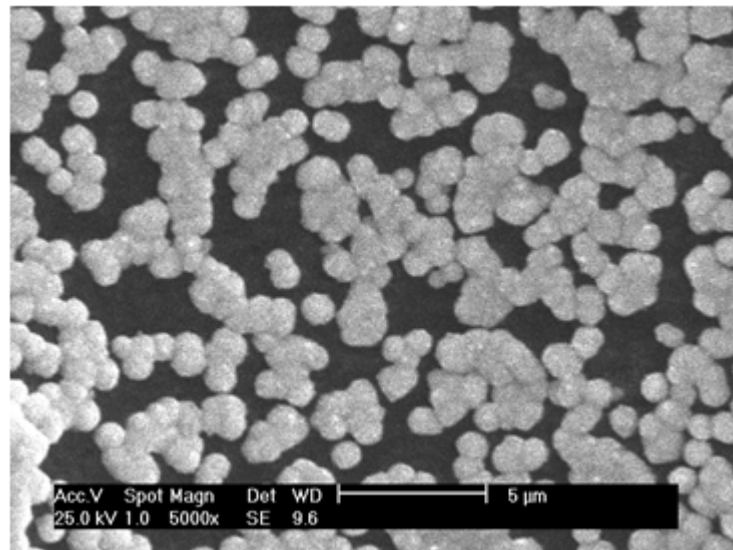
Figure 5.20: Development of Nickel Deposits at $5000X$ Magnification (60 Second Deposition)

The next interval of time examined occurs at 5 minutes of deposition. After 5 minutes of deposition the development of the thin film now encompasses nearly all off the substrate surface (with the exception of void formations), Figure 5.21. Figure 5.22 and 5.23 present the growth of the film at $1000X$ and $5000X$ magnification, respectively. From these figures it can be determined the majority of growth sites originating as nucleation have grown to their maximum in plane dimensions and subsequent growth can only occur as an increase in thickness. This maximum deposit size is approximately 1 to 2 microns.
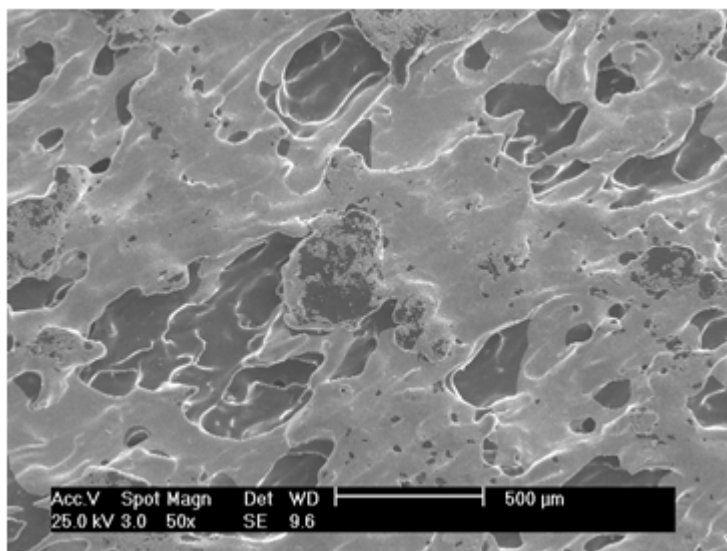
Figure 5.21: Development of Nickel Deposits at 50X Magnification (5 Minute Deposition)
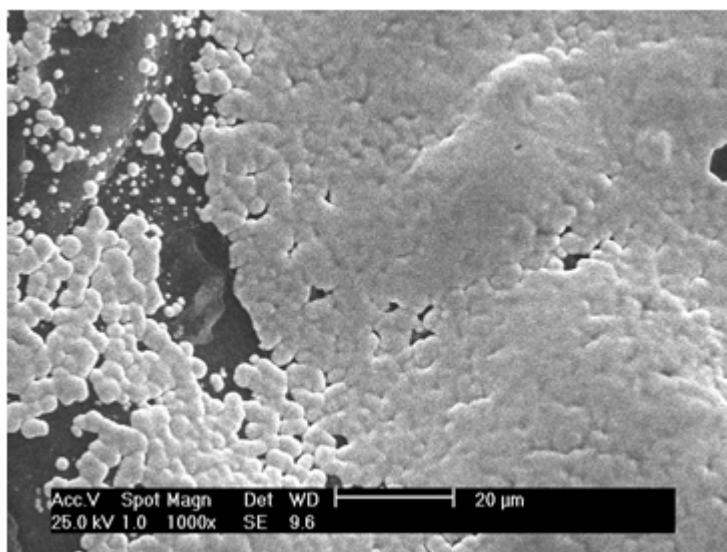
Figure 5.22: Development of Nickel Deposits at 1000X Magnification (5 Minute Deposition)
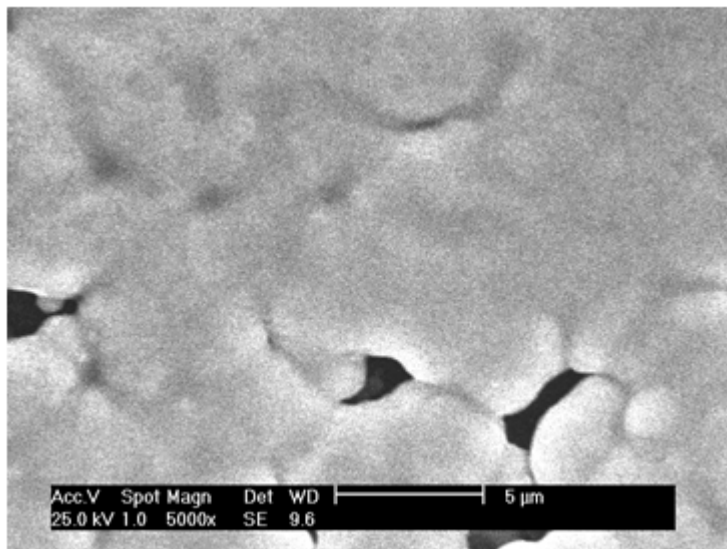
Figure 5.23: Development of Nickel Deposits at $5000X$ Magnification (5 Minute Deposition)

To understand the film growth process after the stage of grain intersection, intervals of 20, 40, 60, and 120 minutes are presented with respect to development of porosity. Figure 5.24 and 5.25 present the SEM images of the films grown for 20 and 40 minutes, respectively. At these stages the continuous film has been established and continued growth occurs resulting in a thicker film on the substrate.
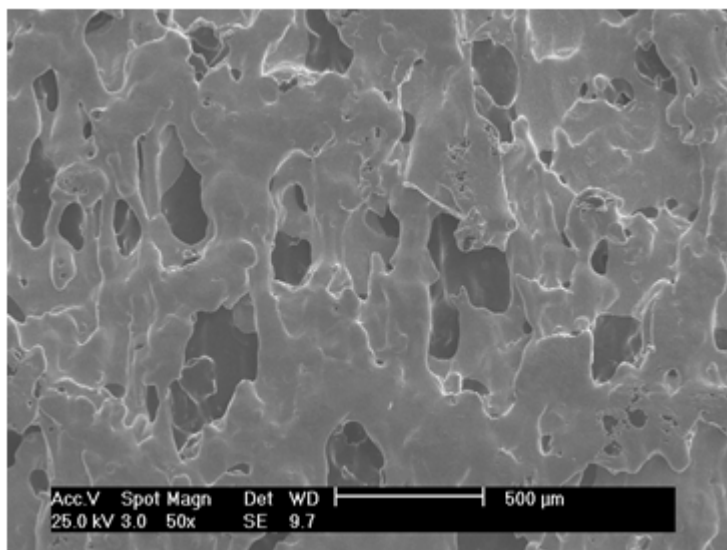
Figure 5.24: Film Growth of Nickel Deposits at $50X$ Magnification (20 Minute Deposition)
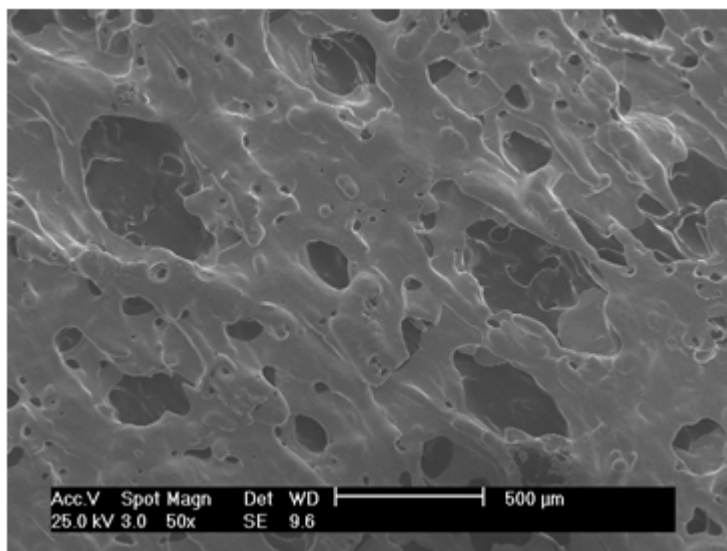
Figure 5.25: Film Growth of Nickel Deposits at $50X$ Magnification (40 Minute Deposition)

Figure 5.26 presents the SEM image of a film grown for 60 minutes (consistent with the 24 samples generated for the main study), while Figure 5.27 corresponds to an electroplating time of 120 minutes.
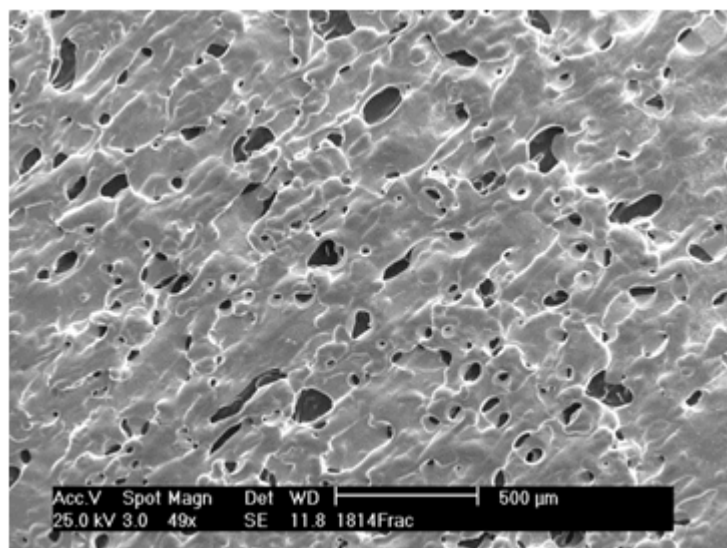
Figure 5.26: Film Growth of Nickel Deposits at $50X$ Magnification (60 Minute Deposition)
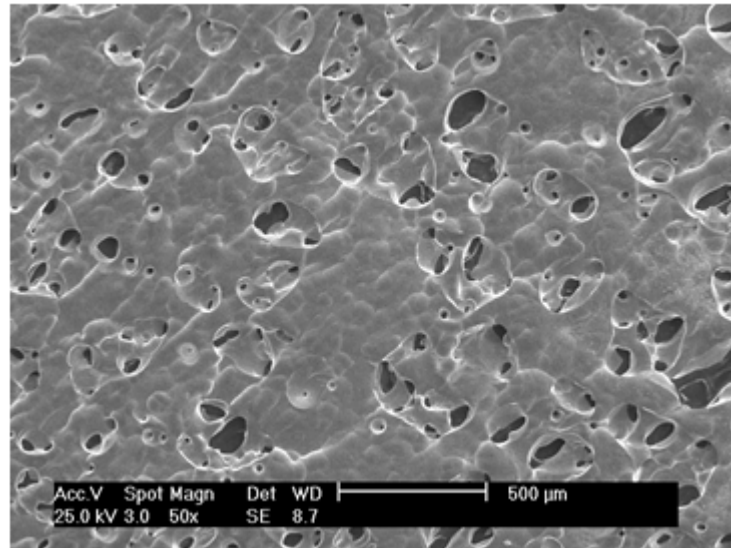
Figure 5.27: Film Growth of Nickel Deposits at 50X Magnification (120 Minute Deposition)

Comparing the SEM images of films deposited for 20, 40, 60, and 120 minutes as shown in the SEM images, it may be observed the void areas appear to be shrinking despite the lack of nickel deposit at that location. This could be a result of the nature of the growth of the film as it moves away from the surface of the substrate. Given local discrepancies that inhibit nucleation of the nickel deposits, growth may occur in an inverted trapezoidal form that shrinks the projection view of the void, Figure 5.28. This presents the possibility that after a sufficient deposition time the voids may become completely encased by the film growth.
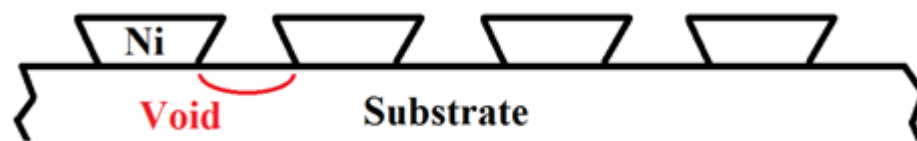
Figure 5.28: Trapezoidal Growth pattern of Film

5.8   Instrumented Indentation

Instrumented indentation is employed to measure key mechanical properties of the deposited films. The equipment used to collect this data is a CSM Nano-Indentation Tester, Figure 5.29, serial number 06-190, coupled with the software "Indentation 3.80.06". The indenter tip used is a Berkovich style diamond tip reference B-I71. The equipment is calibrated against a solid copper sample with a Young's Modulus of 117 GPa.
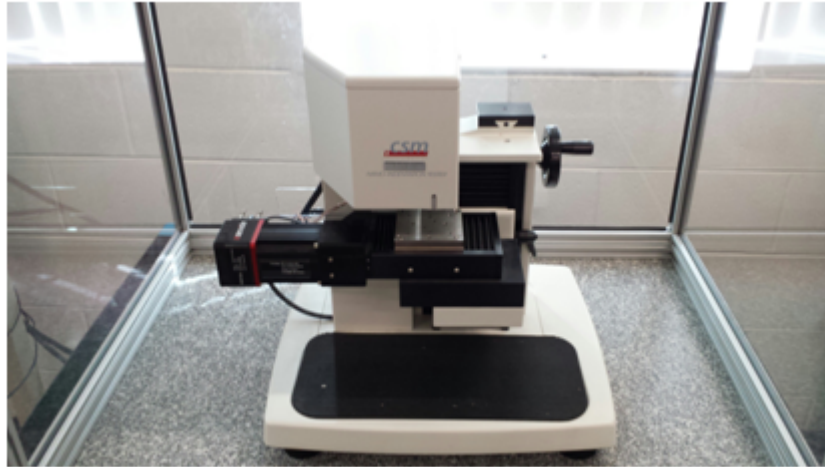
Figure 5.29: CSM Nano-Indentation Tester

As per CSM recommendation key measurement collection parameters are set to derive the most accurate and precise results. The approach speed of the indentation tip is set to 4,000 nm/min. The delta slope for contact fixed at 75% (this is used in the determination of when the indenter tip has made contact with the sample surface). The profile generated for the indentation is a linear program with a loading and unloading rate of 25 mN/min with a 10 second pause at the maximum depth of 1000 nm. The dwell time is incorporated to account for any viscoelastic properties of the film. Figure 5.30 presents a typical profile generated during the indentation process.
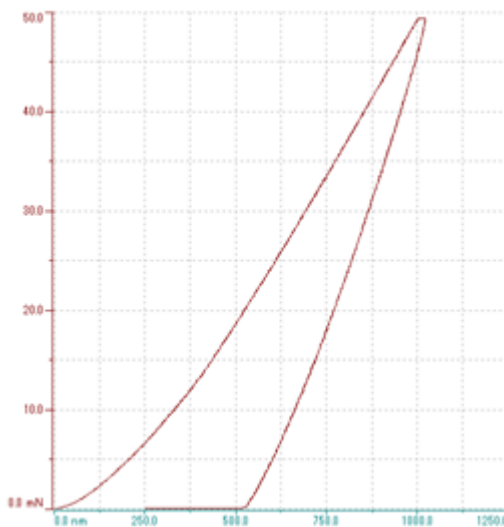
Figure 5.30: Example of Indentation Curve

Ideally the indenter tip would intercept the surface of the film at a location unaffected by changes in gradient or local discrepancies, as this produces the most accurate results. Figure 5.31 depicts such an

indent located on the surface of the film. This particular indent has occurred on a relatively flat area of the film, far removed from any voids or other discrepancies that could alter the data collection process. However, this is not always the case.
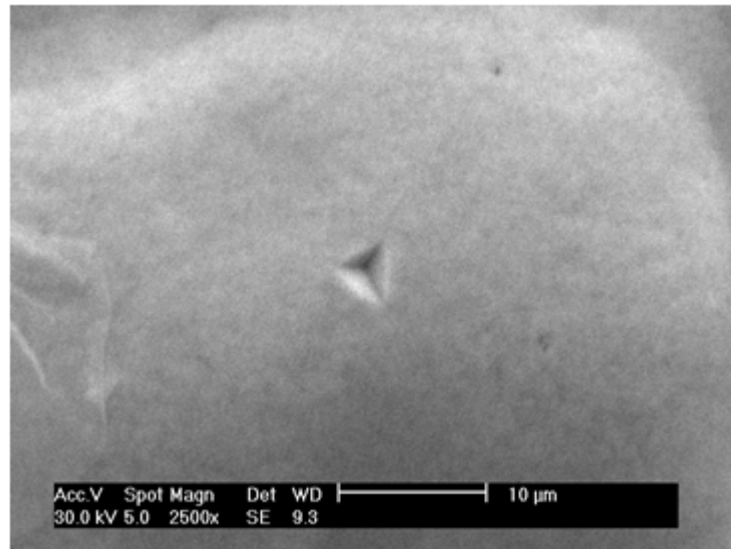
Figure 5.31: Example of Indent as imaged by SEM at $2500X$ Magnification

Due to surface topography variations and discontinuities of the deposited film several indentations are preformed on each sample to determine an accurate mean. Given the surface morphology of the films some data is removed from the analysis due to poor performance of the indentation process. This can be caused by numerous factors including the indenter tips relative location to a void that can disrupt the loading and unloading profile. This erroneous data is often easy to identify by viewing the loading profile. Figure 5.32 presents such a profile that was removed from the analysis due to the indication of a poor indent. Notice the abrupt change of slope during the loading cycle, indicative of incorrect surface contact detection.
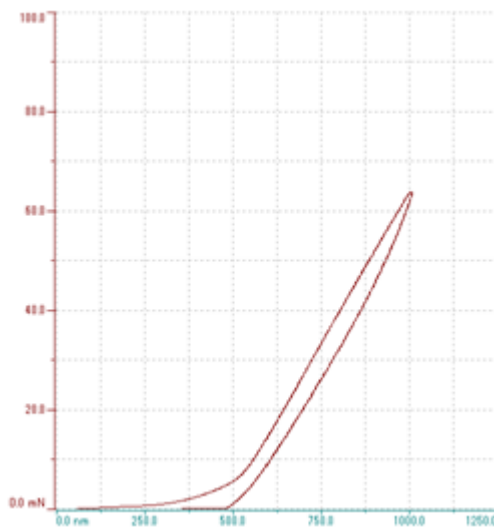
Figure 5.32: Example of Poor Indentation Curve

For each sample, five indentations are used in the resulting calculations. Five samples are chosen to provide an accurate representation of the samples mechanical properties as well as a determination of consistency among the deposit. Table 5.9 through 5.12 present the Young's Modulus and Hardness data derived from the copper samples, respectively. While Table 5.13 through 5.16 present the Young's Modulus and Hardness data derived from the nickel samples, respectively.

Table 5.9: Young's Modulus Data for the Copper Film Samples

Sample	C1	C2	C3	C4	C5	C6
Indent 1	52.585	86.979	120.76	105.5	156.07	162.09
Indent 2	48.155	55.987	119.56	110.06	179.99	175.61
Indent 3	45.842	84.699	115.24	105.91	181.45	158.77
Indent 4	46.262	59.939	98.507	115.77	154.21	163.34
Indent 5	60.682	57.259	127.72	146.05	173.31	167.23

Table 5.10: Young's Modulus Data for the Copper Film Samples, cont

Sample	C7	C8	C9	C10	C11	C12
Indent 1	180.09	185.22	182.42	259.36	207.16	252.42
Indent 2	169.94	188.36	183.63	265.7	206.2	264.87
Indent 3	176.48	176.52	180.56	245.13	215.88	281.45
Indent 4	183.61	198.08	190.81	275.28	224.49	245.93
Indent 5	165.25	192.23	180.48	260.09	218.5	320.24

The first statistical analysis preformed to characterize this data is an Analysis of Variance (ANOVA) study to determine which factors are statistically significant. An ANOVA analysis is completed to compare the means of the samples (within each electroplating parameter category) to the overall mean.

Table 5.11: Hardness Data for the Copper Film Samples

Sample	C1	C2	C3	C4	C5	C6
Indent 1	7319.3	111750	49829	43755	21865	97801
Indent 2	39283	53086	38752	63836	38509	102420
Indent 3	15274	148850	54.298	58728	79247	99605
Indent 4	25921	46411	58982	44462	90449	82192
Indent 5	27173	40149	52372	57053	49300	75741

Table 5.12: Hardness Data for the Copper Film Samples, cont

Sample	C7	C8	C9	C10	C11	C12
Indent 1	68432	126440	49543	232210	127870	93252
Indent 2	27701	96824	54107	79365	66523	81706
Indent 3	66442	127060	34429	202370	70527	108500
Indent 4	55873	144030	49286	201760	77810	114500
Indent 5	61158	132480	52948	21332	66060	211660

By comparing and analyzing the sources of variation, a determination on the significance of each factor (as well as the interaction between the factors) can be presented as a likelihood of significance. Throughout this analysis the confidence level will be set at 95%. The first analysis examines the Young's Modulus and Hardness results from the copper film samples utilizing a General Linear Model ANOVA statistical analysis, Figure 5.33 and 5.34, respectively.

General Linear Model: Youngs Modulus versus Duty Cycle, Current Density

```
Factor            Type    Levels  Values
Duty Cycle        fixed        4  25, 50, 75, 100
Current Density   fixed        3  5, 10, 15


Analysis of Variance for Youngs Modulus, using Adjusted SS for Tests

Source                       DF  Seq SS  Adj SS  Adj MS       F      P
Duty Cycle                    3   25618   25618    8539   48.87  0.000
Current Density               2  212370  212370  106185  607.68  0.000
Duty Cycle*Current Density    6   18639   18639    3106   17.78  0.000
Error                        48    8387    8387     175
Total                        59  265014


S = 13.2188   R-Sq = 96.84%   R-Sq(adj) = 96.11%
```

Figure 5.33: ANOVA Analysis of Young's Modulus resulting from Copper Films

Table 5.13: Young's Modulus Data for the Nickel Film Samples

Sample	N1	N2	N3	N4	N5	N6
Indent 1	31.234	61.629	97.783	108.21	68.059	107.46
Indent 2	29.68	71.471	88.864	101.57	61.491	101.39
Indent 3	30.714	80.401	81.942	109.68	70.964	86.7
Indent 4	31.938	89.019	75.28	114.53	63.113	108.73
Indent 5	32.296	95.556	90.48	123.09	72.179	99.728

Table 5.14: Young's Modulus Data for the Nickel Film Samples, cont

Sample	N7	N8	N9	N10	N11	N12
Indent 1	121.9	101.44	78.048	163.61	146.69	142.41
Indent 2	113.52	111.92	69.659	124.4	148.21	143.92
Indent 3	137.41	154.42	75.966	95.067	117.38	152.8
Indent 4	127.61	143.54	71.523	105.32	131.36	143.67
Indent 5	111.39	149.04	81.809	112.99	151.1	150.73

General Linear Model: Hardness versus Duty Cycle, Current Density

```
Factor           Type   Levels  Values
Duty Cycle       fixed       4  25, 50, 75, 100
Current Density  fixed       3  5, 10, 15


Analysis of Variance for Hardness, using Adjusted SS for Tests

Source                      DF       Seq SS       Adj SS       Adj MS      F      P
Duty Cycle                   3  43832023926  43832023926  14610674642  10.65  0.000
Current Density              2  26432245740  26432245740  13216122870   9.63  0.000
Duty Cycle*Current Density   6  10342046177  10342046177   1723674363   1.26  0.295
Error                       48  65843015415  65843015415   1371729488
Total                       59  1.46449E+11
```

Figure 5.34: ANOVA Analysis of Hardness resulting from Copper Films

From the ANOVA analysis several key results can be obtained. Concerning the Young's Modulus it is determined that not only are the duty cycles and current densities significant (as $p < .05$), but also the interaction of the duty cycle and current density is significant at the 95% level. Concerning the Hardness data it is determined the duty cycles and current densities are significant, however the interaction between the two is not (as $p > .05$). The second analysis examines the Young's Modulus and Hardness results from the nickel film samples utilizing the same General Linear Model ANOVA statistical analysis, Figure 5.35 and 5.36, respectively.

Table 5.15: Hardness Data for the Nickel Film Samples

Sample	N1	N2	N3	N4	N5	N6
Indent 1	33564	42822	137940	108890	80753	44316
Indent 2	34586	69336	68557	94909	96000	63552
Indent 3	37263	57428	151650	138260	109460	51689
Indent 4	68631	87736	106170	96264	68245	179930
Indent 5	54634	116250	161120	86024	17863	127910

Table 5.16: Hardness Data for the Nickel Film Samples, cont

Sample	N7	N8	N9	N10	N11	N12
Indent 1	128120	132330	73797	192740	83424	108960
Indent 2	117550	78678	111090	123600	90613	103120
Indent 3	180380	369390	77181	146830	106260	103620
Indent 4	121080	595180	57729	220030	170490	58604
Indent 5	81865	207520	66583	206880	28989	48324

General Linear Model: Youngs Modulus versus Duty Cycle, Current Density

```
Factor            Type   Levels  Values
Duty Cycle        fixed       4  25, 50, 75, 100
Current Density   fixed       3  5, 10, 15


Analysis of Variance for Youngs Modulus, using Adjusted SS for Tests

Source                     DF   Seq SS   Adj SS   Adj MS      F      P
Duty Cycle                  3  43931.8  43931.8  14643.9  85.62  0.000
Current Density             2  19162.2  19162.2   9581.1  56.02  0.000
Duty Cycle*Current Density  6    728.1    728.1    121.3   0.71  0.644
Error                      48   8209.2   8209.2    171.0
Total                      59  72031.2
```

Figure 5.35: ANOVA Analysis of Young's Modulus resulting from Nickel Films

General Linear Model: Hardness versus Duty Cycle, Current Density

```
Factor            Type   Levels  Values
Duty Cycle        fixed       4  25, 50, 75, 100
Current Density   fixed       3  5, 10, 15


Analysis of Variance for Hardness, using Adjusted SS for Tests

Source                     DF       Seq SS       Adj SS       Adj MS     F      P
Duty Cycle                  3  60458677198  60458677198  20152892399  4.17  0.011
Current Density             2  30742516057  30742516057  15371258029  3.18  0.051
Duty Cycle*Current Density  6  1.16840E+11  1.16840E+11  19473405135  4.03  0.002
Error                      48  2.32148E+11  2.32148E+11   4836407794
Total                      59  4.40189E+11
```

Figure 5.36: ANOVA Analysis of Hardness resulting from Nickel Films

The results of the ANOVA Analysis for the Young's Modulus of the nickel samples indicate that

both the current density and duty cycle show a significant role concerning the resulting film's Young's Modulus. However, the interaction between the factors is not significant. The results from the Hardness analysis indicate that the duty cycle is significant, whereas the current density may or may not be at the 95% level, (as the p value is equal to .051) for the remainder of the research it will be considered significant. Additionally, the interaction between the duty cycle and current density is believed to be significant.

While the ANOVA analysis determined the significance of each factor, it does not resolve relationships with respect to the individual factors. Presented next are plots of the mean values for both Young's Modulus and Hardness across both copper and nickel. This is done to provide a relative comparison amongst the various duty cycles, current densities, and materials. Linear trend lines are added to the plots to allow for easier recognition of trends. First plotted are the Young's Modulus results for both copper and nickel. Figure 5.37 presents the data analyzed against the various duty cycles, while Figure 5.38 presents the data analyzed against the various current densities.
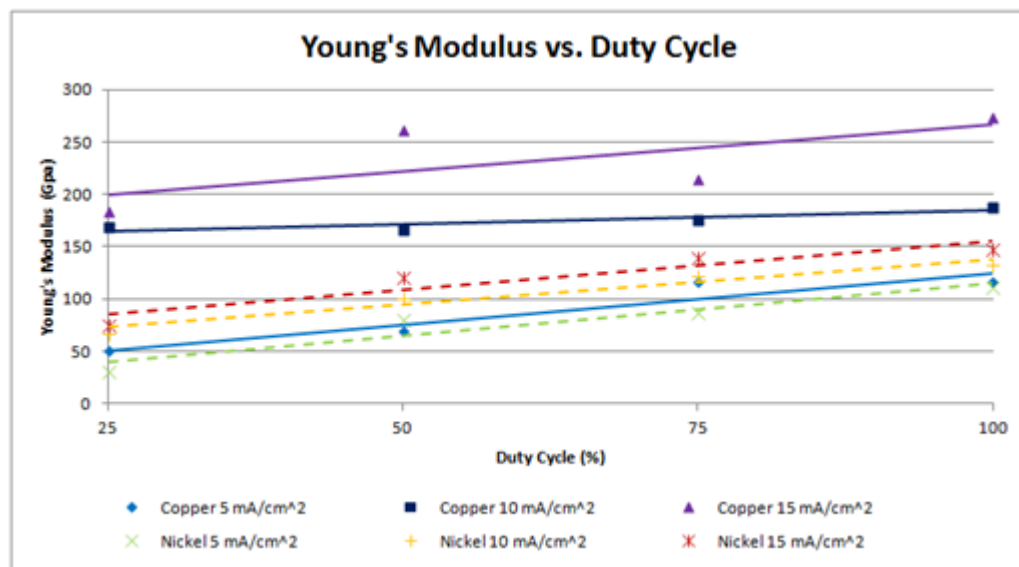

Figure 5.37: Young's Modulus Results plotted against the Various Duty Cycles

Figure 5.38: Young's Modulus Results plotted against the Various Current Densities

Examination of these plots revels a great deal of information. An increase in Youngs Modulus and Hardness is correlated to an increase in duty cycle as well as current density. The Copper film's Young Modulus can be increased by 230% by increasing the current density and duty cycle, hardness by 350%. Similarly for the Nickel films the Young's Modulus can be increased by 275%, hardness by 300%. This results present an outstanding increase from a minimum current density/minimum duty cycle film, to a maximum current density/maximum duty cycle film.

In addition it is determined the data conforms well to a linear trend line. Indicating Young's Modulus is a linear function of current density as well as duty cycle (at least in the ranges presented). This trend appears as a positve slope for both copper and nickel. An increase in duty cycle and/or current density, correlates to a direct increase in the samples Young's Modulus, an important determination in the characterization of the thin metallic films. Additionally, copper exhibits a higher Young's Modulus when compared to nickel for each duty cycle/current density combinations. This is contrary to the bulk properties relationship of the two materials (bulk copper Young's Modulus = 117 GPa, bulk nickel Young's Modulus = 170 GPa), indicitive of a scaling factor that alters the materials mechanical properties at the micro-scale. Plotted next are the Hardness results for both copper and nickel. Figure 5.39 presents the data analyzed against the various duty cycles, while Figure 5.40 presents the data analyzed against the various current densities.
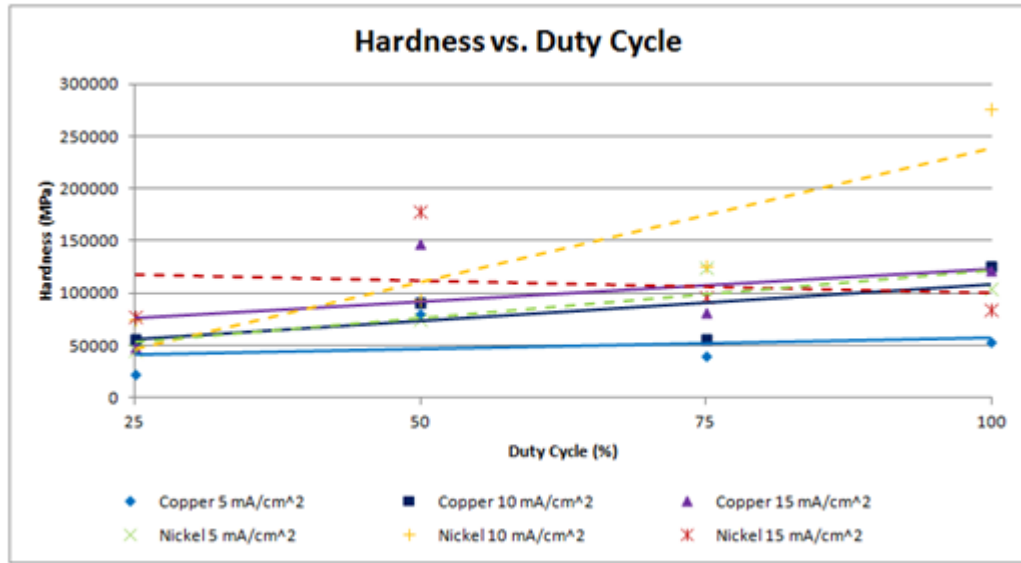
Figure 5.39: Hardness Results plotted against the Various Duty Cycles

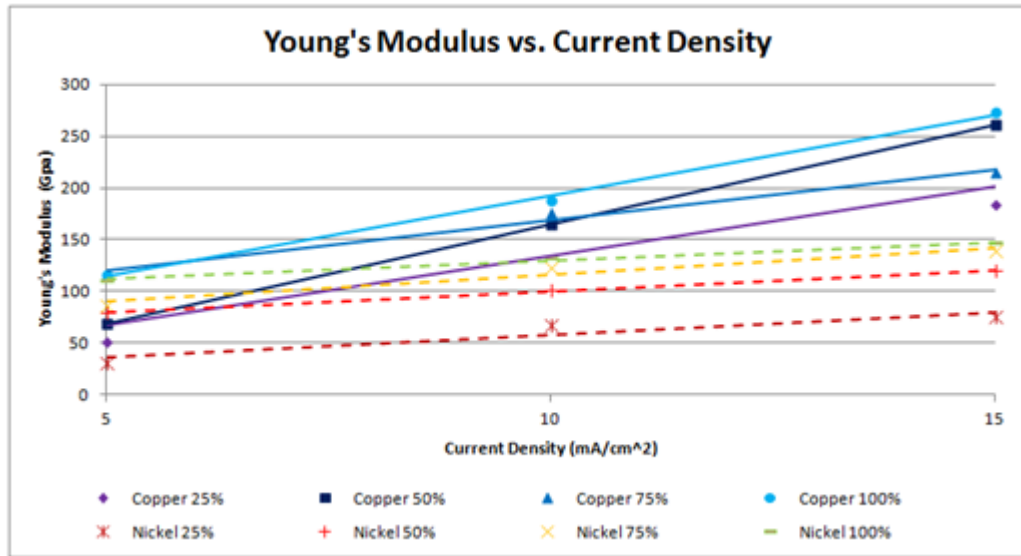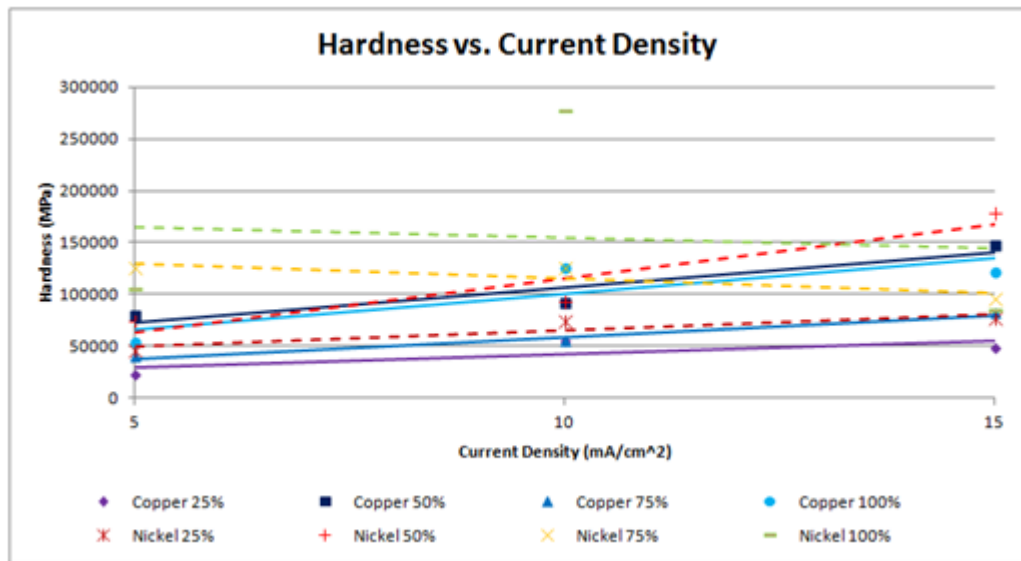Figure 5.40: Hardness Results plotted against the Various Current Densities

Once again the data is fitted to linear trend lines, which appear to fit the data well, with few exceptions. In general the hardness of the film increases with an increase in duty cycle and or current density. And while there is overalapping of the data between copper and nickel, the nickel films in general exhibt a higher hardness when compared to the copper films, consistent with the relationship of the bulk material mechanical properties.

Correlating the nanoindentation results to the SEM data shows that the relatively larger grain struc-

tures of the Copper deposits are related to a higher Young's Modulus and lower Hardness when compared to the Nickel deposits. The Nickel deposits with the smaller, featureless, grains correspond to a relatively higher hardness. Consistent with mechanical theory in which smaller grains (which yields an increase in grain boundary density) have increased mechanical properties such as wear properties, fracture resistance, as well as the observed Hardness. This trend continues within the Copper samples wherein it is found an increase in duty cycle (and thus a decrease in grain size) results in a higher hardness value.

The results covering the nanoindentation data may include significant error concerning the lower duty cycle samples wherein it was found the actual current density may deviate from the ideal current density. This may explain the contradiction to the results of the work completed by Luo et al wherein it was found that the Young's Modulus of electroplated Nickel actually decreases with an increase in current density [34].

To ascertain a measurement for the adhesion of the films to the substrate a preliminary test was conducted to measure the force required to mechanically remove a deposit from the substrate. In this experiment a wire is fixed to the center of the deposits (utilizing a high strength epoxy adhesive), Figure 5.41, and then the wires are connected to a tensile testing machine with an inline force gauge. The polymer substrate is held stationary while a force is applied to the wires until the point of failure (part of all of the deposit is removed from the substrate). Preliminary results measured a force of 27.2 Newtons required to generate a failure of a deposit.

Figure 5.41: Lead Wires attached to Polymer Substrate and Tensile Machine (not shown)

This chapter has presented several key findings on the determination of the characterstics of the

metallic thin films. SEM analysis concluded the copper films feature prominate grain structures on the order of 500 nm to 5000 nm, whereas nickel deposits display a featureless topography. The SEM data coupled with EDS analysis concluded the descrepencies in the film are infact voids contribuiting to the overall porosity of the film. Of which the nickel films present a higher rate of when compared to the copper films.

The nanoindentation results when analyzed using ANOVA statistical analysis determined the significance of the duty cycles as well as the current densities as they effect the resulting deposit's mechanical properties. Both Young's Modulus and Hardness are found to be linear functions, proportional to the duty cycle and current density. Copper is found to have a relatively higher Young's Modulus for a given set of electoplating parameters, while nickel has a slightly higher hardness. The results of these analyses will be concluded in the next chapter in which deteriminations on the thin films as well as reccomendations will be made.

Chapter 6

Conclusions

This chapter concludes the Thesis with the presentation of the main results derived in the course of this research. Providing a comprehensive analysis into the optimization of parameters, pertaining to the electrodeposition of a metallic film onto a selectively resistive polymeric substrate. Proposed selection considerations are discussed as they pertain to various product applications and manufacturing methods. Lastly, recommendations are then made relative to the advancement of research into this growing field.

6.1   Research Results

Thermoplastics benefit from a wide variety of potential forming operations. The usage of elevated temperature extrusion was chosen for simplicity as well as the option of variable output geometries. This method proved successful as rod samples were initially formed, before the finial wafer shape was chosen for the remainder of the analysis. Post forming operations were also experimented with to determine validity, such as the use of vacuum deposition of aluminum to enhance the conductivity of the sample in select areas. While this operation was beneficial when the distance between the cathode terminal of the power supply and the area to be deposited was large (as it was with the rod samples), it was shown unnecessary for the wafer samples. Other operations examined include the compression of the polymer samples, post extrusion. Compression of the extrudate for an extended period of time was observed to increase the ductility of the sample, allowing greater degrees of bending to occur before fracture (failure) occurred. This phenomenon is also observed substituting the compression stage for a rolling oberation. It is this combination of forming (extrusion and rolling) operations chosen to manufacture the substrates used in this research. Although forming operations should be based on optimized parameters for each individual use of this polymeric material.

In the course of experimentation it is often beneficial to perform simulations, either in an effort to

confirm numerical data, or to validate and further explain results. In this research, one such simulation was used to study the effect of film porosity as it relates to extrinsic stressing. Electroplated deposits were determined to exhibit varying levels of porosity (primarily nickel films featured greater levels of porosity than copper films); the result of this porosity must be examined as it relates to the performance criteria previously defined. Namely the distribution of stresses in the film, which for a continuous deposit is generally linear and consistent. For the porous model stresses are shown to vary based on the geometric relation to local vacancies. These local stressors often indicate regions first to succumb to failure, thus it is desired to minimize porosity in the film, which favors the copper film deposits.

The second simulation performed aimed to provide a comprehensive understanding of the performance of a nanoindentation test into a thin film atop a substrate. Primarily the distribution of displacement as it relates to indenter tip depth. To accurately determine the mechanical properties of the film it is required all material displacement is localized to the film. Thus a maximum indenter tip depth was determined (13.76% of total film thickness), and all subsequent instrumented indentation tests were performed within the limits of this parameter.

To facilitate the analytical experimentation of the thin film parameters, 24 samples are generated. The samples undergo electrodeposition with varying duty cycles, current densities, as well as constituent film material. The 24 samples prepared cover four levels of duty cycle (25%, 50%, 75%, and 100%), three levels of cathodic current density (5 mA/cm^2, 10 mA/cm^2, and 15 mA/cm^2), and two materials (copper and nickel). The deposition time for all samples is 60 minutes, producing films with theoretical thicknesses ranging from 8.35 microns to 36.62 microns. The deposited metallic thin films experience excellent coverage of the selected areas (with the exception of the samples deposited under low current density and low duty cycle parameters). Electroplating is shown to be a viable option for the deposition of a metallic film. Through the use of masking, selectable geometries are possible for the deposition areas.

Characterization of the samples is completed with respect to the goal of optimization. Tools such as Scanning Electron Microscopy (SEM) and Energy Dispersive X-Ray Spectrometer (EDS) are used to determine relative levels of porosity in the films as well as grain growth and size. This led to the conclusion that throughout every duty cycle the copper film presents a greater level of homogeneity with fewer discrepancies. The nickel film exhibits a porous deposit with many vacancies. These vacancies are confirmed through the EDS analysis in which high concentrations of carbon and a lack of metallic elements in the vacancy area confirmed it is the polymer that appears as the discrepancies on the images.

SEM is also utilized for grain size determination in which it is found copper has relatively large, well defined grains. Nickel however, exhibits smooth featureless deposits with a relatively smaller grain size. To better understand the nature of the grains comprising the nickel film, various electrodeposition

times are studied to examine the grain growth. The results of which show the initial nucleation process, wherein small round sites begin to form across the surface of the substrate. These sites continue to grow and eventually intersect one another. From this point on growth occurs primarily in the direction perpendicular to the substrate surface, resulting in an increase in film thickness. Some areas however neglected to allow for the formation of nucleation sites. It is these areas that will result in eventual porosity of the film as they inhibit the deposition.

To continue the characterization of the deposited films instrumented indentation is utilized to measure key mechanical properties, namely Young's Modulus and Hardness. An appropriate profile is chosen and the maximum indenter tip depth (as determined via simulations) is selected as 1000 nm. Difficulties arise as a result of the topology of the film on which the indent occurs. Discrepancies such as voids and gradient variations disrupt the measurement collection process and result in erroneous readings. Therefore multiple measurements are collected per sample to indentify accurate values for the films Young's Modulus and Hardness.

Results from the nanoindentation are complied and analyzed using an ANOVA statistical analysis to determine the significance of each factor. It is determined that within a given material, mechanical properties rely heavily on the depositions current density and duty cycle. It is found that a positive correlation exists between the current density/duty cycle and Young's Modulus/Hardness. An increase in either factor results in a proportional increase in the mechanical property values. With respect to the individual material results, copper was found to have a higher Young's Modulus (for equivalent deposition parameters) while nickel exhibited a higher Hardness (for equivalent deposition parameters).

6.2   Recommendations for Future Research

Throughout this research copper and nickel films were successful deposited onto a nanoengineered polymer substrate. While the films provide excellent electrical conductivity (relative to the semi-conductive substrate) the mechanical properties of the depositions can vary greatly based on the electroplating parameters. Therefore the determination of the preeminent material/parameter combination is not an inherit truth, rather the selection of which is to be based on the specific commercial/industrial application requirements.

Material selection based on mechanical properties is a well documented practice revolutionized by the work of Michael Ashby. In the case of selecting the correct material/parameter for electrodeposition careful attention should be paid to the variations encountered with regards to the film's hardness and Young's Modulus. It was found the range of Young's Modulus is 50 to 270 GPa for copper and 30 to 150 GPa for nickel. Additionally hardness ranges from 23000 to 150000 MPa for copper and 45000 to

275000 MPa for nickel, Figure 6.1. This range of mechanical properties allows for direct selection of the most well suited film for each particular application.
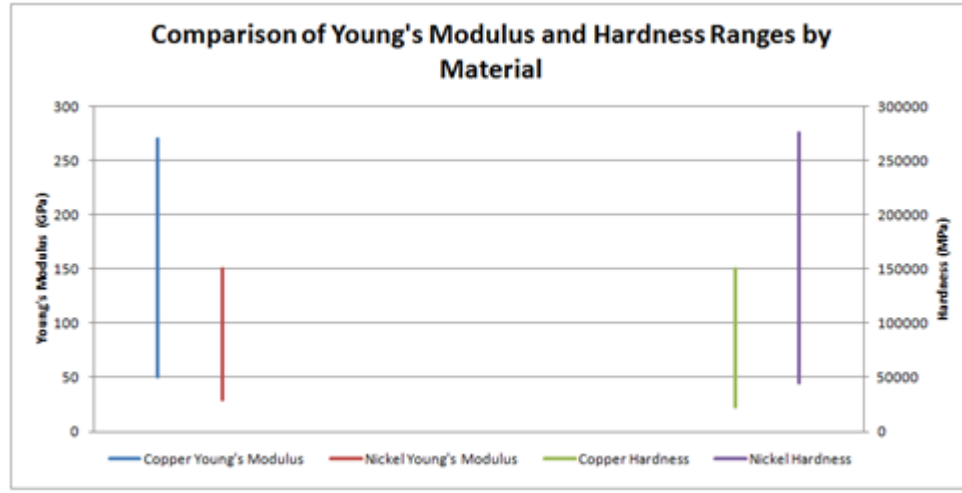

Figure 6.1: Range of Material Mechanical Properties for Copper and Nickel

In applications where wear resistance is a concern the higher hardness values of the nickel film may be preferential. Whereas the higher Young's Modulus of the copper deposits would require a higher load to elastically deform the film, a potential benefit for select applications.

Other material/parameter selection considerations beyond the mechanical properties include the morphology and topology of the deposits. Wherein it was discovered the nickel exhibited a relatively porous deposit. As shown in the simulations, porosity can introduce higher local stressors which can promote debonding from the substrate. Therefore in applications where extrinsic flexural stressors will be applied, the copper deposits, with low porosity, would be preferential. The ability to selectively control grain size has large implications in terms of fracture resistance, as a film with smaller grains has a greater density of grain boundary interfaces which impede fracture propagation. Therefore as discussed with the SEM results the higher duty cycle deposits, namely DC (100% Duty Cycle), will exhibit superior fracture resistance.

A wide range of mechanical and morphological properties lends to a wide range of applications. However further research is still required to achieve full benefit of a thin metallic film atop a semi-conductive polymer. The manufacturing methods employed in the generation of the wafer samples left a semi-controlled roughness to the surface. While this roughness increases the surface area and may have aided in adhesions, it affects the topology of the film (as the film contours to the substrate surface). Refinements to the manufacturing of the polymer should including a controllable engineered roughness, based on the requirements of the application.

The specification application of the film through electrodeposition is a robust process that deposits anywhere on the substrate that is exposed to the electrolyte. In the course of this research the relatively simple geometry of the deposits could be achieved by a special fixture. However for complex and or variable geometries a more robust masking technique must be employed. Such as an insulatory film that could be adhered to the polymer before the deposition process. Requirements of the mask include chemical inertness to the electrolyte solution, as well as strong adhesion as to not debond from the substrate.

Further characterization of the deposited films should come in the form of adhesion strength tests. While many of the discussed properties of the film affect adhesion, analytical data regarding the subject is limited to the preliminary results presented. Various experimental methods could be employed to measure and qualitatively determine the various adhesion strengths between the samples. One such study involves the direct adhesion of a force gage to the film, and measuring the force required to separate the film from the substrate. Initial testing of this type was completed by an independent third party and determined the force required to debond the film was in the range of 27 Newtons.

Indepth characterization of the film can be completed by use of an Atomic Force Microscope (AFM) in which a mechanical scanning probe navigates the surface of the sample to produce a 3D image of the deposit. This type of system would be beneficial to better understand the surface topology of the electrodeposits, to provide further correlations between the SEM gather data and the measured mechanical properties. However this measure system was not available during the course of this research.

Concerning future work regarding this research topic attention should be paid to accurately control the actual current supply from the power source to ensure the current density is correct. This will eliminate a large source of error encountered during this research wherein the power supple did not provide the desired current. Electroplating should also be conducted on various substrate materials (silicon for example) to validate the results. Depositing on a substrate with a higher mechanical hardness will also facilitate deeper penetration depths concerning the nanoindentation procedure which can lead to more accurate results.

The application of a thin metallic film atop a nanoengineered substrate has many industrial and commercial applications. From static discharge dispersion in the aerospace industry to antennas incorporated into cellular phone covers. The efforts presented here to determine the optimal material and deposition parameters have shown successful deposition and provided a general characterization of the mechanical and morphological properties. Further research into this field could potentially expand the existing nanoengineered polymer manufacturing methods as well as the properties of the electrodeposited films. Providing increased potential applicational usage in a variety of engineering fields and consumer markets.

References

[1] M. Shulaker, G. Hills, N. Patil, H. Wei, H. Chen, H. Wong, and S. Mitra, "Carbon nanotube computer." [Online]. Available: http://www.nature.com/nature/journal/v501/n7468/full/nature12502.html

[2] J. Ribeiro, "Stanford researchers develop first computer using only carbon nanotube transistors." [Online]. Available: http://www.pcworld.com/article/2049460/stanford-researchers-develop-first-computer-using-only-carbon-nanotube-transistors.html

[3] B. Newell, G. Krutz, M. Harmeyer, and M. Holland, "Integrity sensing with smart polymers and rubber components on vehicles."

[4] C. Morris, "Carbon fiber reinforced plastic," *ASME*, August 2013.

[5] M. Crawford, "Cars without combustion," *ASEM*, August 2013.

[6] S. Rawal, J. Brantley, and N. Karabudak, "Additive manufacturing of ti-6al-4v alloy components for spacecraft applications."

[7] V. Fleury, W. Watters, L. Allam, and T. Devers, "Rapid electroplating of insulators."

[8] J. B. Mohler, "Electroplating and related processes," 1969.

[9] A. Sanders, *Electroplating.* International Textbook Company, 1950.

[10] L. Romankiw and E. OSullivan, "Plating techniques handbook of microlithography, micromachining, and microfabrication," 1997.

[11] G. A. Di Bari, "Electrodeposition of nickel," *Modern electroplating, 4th edn. Wiley, New York*, pp. 139–200, 2000.

[12] N. Qu, D. Zhu, K. Chan, and W. Lei, "Pulse electrodeposition of nanocrystalline nickel using ultra narrow pulse width and high peak current density," *Surface and Coatings Technology*, vol. 168, no. 2, pp. 123–128, 2003.

[13] D. YFANTIS, S. KAKOS, S. LAMPRAKOPOULOS1, S. DEPOUNTIS, and C. YFANTIS, "Copper electrodeposition on insulators (plastics) using highly conductive polypyrrole films."

[14] M. Ghantasala and D. Sood, "Novel method for electroplating on silicon without the need of a continuous-plating base film," in *Far East and Pacific Rim Symposium on Smart Materials, Structures, and MEMS.* International Society for Optics and Photonics, 1997, pp. 52–58.

[15] ——, "Ion implantation seeding of electroplated permalloy films on silicon," pp. 619–632, 1999.

[16] B. Poon, D. Rittel, and G. Ravichandran, "An analysis of nanoindentation in linearly elastic solids," *International Journal of Solids and Structures*, vol. 45, no. 24, pp. 6018–6033, 2008.

[17] M. VanLandingham, "Review of instrumented indentation," DTIC Document, Tech. Rep., 2003.

[18] Cornell, "Elastic contact analysis." [Online]. Available: http://www.nanoindentation.cornell.edu/Model/elastic_model.htm

[19] *CSM Instruments: Indentation Software manual.*

[20] N. Sakharova, M. Oliveira, J. Antunes, and J. Fernandes, "On the determination of the film hardness in hard film/substrate composites using depth-sensing indentation," *Ceramics International*, vol. 39, no. 6, pp. 6251 – 6263, 2013. [Online]. Available: http://www.sciencedirect.com/science/article/pii/S0272884213000783

[21] M. Müller, B. Krause, B. Kretzschmar, and P. Pötschke, "Influence of feeding conditions in twin-screw extrusion of pp/mwcnt composites on electrical and mechanical properties," *Composites Science and Technology*, vol. 71, no. 13, pp. 1535–1542, 2011.

[22] B. Krause, P. Pötschke, and L. Häußler, "Influence of small scale melt mixing conditions on electrical resistivity of carbon nanotube-polyamide composites," *Composites Science and Technology*, vol. 69, no. 10, pp. 1505–1515, 2009.

[23] P. Pötschke, B. Krause, S. Buschhorn, U. Köpke, M. Müller, T. Villmow, and K. Schulte, "Improvement of carbon nanotube dispersion in thermoplastic composites using a three roll mill at elevated temperatures," *Composites Science and Technology*, vol. 74, pp. 78–84, 2013.

[24] C. Rauwendaal, *Polymer Extrusion*, 3rd ed. Hanser Publishers.

[25] L. Freund and S. Suresh, *Thin Film Materials: Stress, Defect Formation and Surface Evolution.* Press Syndicate of the Univeristy of Cambridge.

[26] R. Cagliero and G. Maizza, "Modeling of vickers indentation of tial alloys," in *Excerpt from the Proceedings of the COMSOL Conference, Paris*, 2010.

[27] M. Chandrasekar and M. Pushpavanam, "Pulse and pulse reverse platingconceptual, advantages and applications," *Electrochimica Acta*, vol. 53, no. 8, pp. 3313–3322, 2008.

[28] W. Kleinekathöfer and C. Raub, "Die abscheidung von nickel mit pulsierendem strom," *Surface Technology*, vol. 7, no. 1, pp. 23–34, 1978.

[29] A. Sonin, "Jet impingement systems for electroplating applications: mass transfer correlations," *Journal of The Electrochemical Society*, vol. 130, no. 7, pp. 1501–1505, 1983.

[30] T. Clyne, "Residual stresses in thick and thin surface coatings."

[31] B. Bhushan, "Adhesion and stiction: mechanisms, measurement techniques, and methods for reduction," *Journal of Vacuum Science & Technology B*, vol. 21, no. 6, pp. 2262–2296, 2003.

[32] M. F. Ashby, "Materials selection in mechanical design. 1999," 2002.

[33] D. Jeong, F. Gonzalez, G. Palumbo, K. Aust, and U. Erb, "The effect of grain size on the wear properties of electrodeposited nanocrystalline nickel coatings," *Scripta Materialia*, vol. 44, no. 3, pp. 493–499, 2001.

[34] J. Luo, A. Flewitt, S. Spearing, N. Fleck, and W. Milne, "Young's modulus of electroplated ni thin film for mems applications," *Materials Letters*, vol. 58, no. 17, pp. 2306–2309, 2004.